INTERNATIONAL JOURNAL FOR NUMERICAL METHODS IN FLUIDS, VOL. 7, 489–520 (1987)

A TAYLOR WEAK-STATEMENT ALGORITHM FOR HYPERBOLIC CONSERVATION LAWS

A. J. BAKER AND J. W. KIM

Department of Engineering Science and Mechanics, University of Tennessee, Knoxville, TN 37996-2030 U.S.A.

SUMMARY

Finite element analysis, applied to computational fluid dynamics (CFD) problem classes, presents a formal procedure for establishing the ingredients of a discrete approximation numerical solution algorithm. A classical Galerkin weak-statement formulation, formed on a Taylor series extension of the conservation law system, is developed herein that embeds a set of parameters eligible for constraint according to specification of suitable norms. The derived family of Taylor weak statements is shown to contain, as special cases, over one dozen independently derived CFD algorithms published over the past several decades for the high speed flow problem class. A theoretical analysis is completed that facilitates direct qualitative comparisons. Numerical results for definitive linear and non-linear test problems permit direct quantitative performance comparisons.

KEY WORDS CFD Algorithm Weak Statement Hyperbolic Parabolic Dissipation Dispersion

INTRODUCTION

Research on finite element analysis in computational fluid dynamics (CFD) over the past decade has focused on derivation and definition of suitable weak statements for the Navier–Stokes equations for high speed flow. The Navier–Stokes CFD problem class is characterized by large Reynolds (Peclet) number, so that the resulting equation system approximates (over a large portion of the solution domain) the inviscid hyperbolic conservation law system termed the Euler equations. The earliest finite element developments include those of Wahlbin,[1] Dendy[2] and Raymond and Garder[3] for linear scalar first-order hyperbolics. The family of Petrov–Galerkin algorithms followed,[4–6] as well as the penalty–Galerkin algorithm of Baker and Soliman[7] and the characteristic–Galerkin method.[8] In every instance, for a given space of trial functions, a non-Galerkin test space was identified that yielded a dissipative modification to the parent Galerkin algorithm. Invariably, one of the additional terms thus generated involved a second spatial derivative that yielded an 'artificial viscosity' term, with the action of smoothing the short wavelength dispersion error inherent in approximate solutions of the Euler equations.

Of importance to the current development, and in formulational distinction to those previously cited algorithms, Donea[9] developed the 'Taylor–Galerkin' algorithm wherein the weak statement was formed on a Taylor series expansion of the unsteady equation, with higher-order derivatives re-expressed in terms of derivatives of the flux vector of the first-order hyperbolic conservation law (system). The interchanging of weak statement and Taylor series immediately generated perspective into independently derived finite element CFD algorithms for problem classes ranging from transonic potential flow to high-speed Navier–Stokes.[10]

The richness of this formulational procedure is expanded herein to derive and evaluate a

0271–2091/87/050489–32$16.00

Received 6 February 1986
Revised 5 September 1986

generalized family of finite element CFD algorithms using the classical Galerkin test space constraint applied to a Taylor weak statement for first-order hyperbolics. The developed algorithm is verified to contain as special cases over a dozen independently derived finite difference and finite element algorithms. Definitive steady and unsteady, linear and non-linear model problem test cases are solved to critically compare the relative performances of these algorithms, in concert with a complete linearized theoretical analysis for qualitative comparisons.

PROBLEM STATEMENT

Hyperbolic conservation law system

Consider the homogeneous hyperbolic conservation law system

$$L(q) = \frac{\partial q}{\partial t} + \frac{\partial f_j}{\partial x_j} = \frac{\partial q}{\partial t} + \frac{\partial \mathbf{f}(q)}{\partial \mathbf{x}} \equiv q_t + \mathbf{f}_\mathbf{x} = 0, \tag{1}$$

where boldface indicates a vector field. In equation (1), $\mathbf{x}$ spans the appropriate n-dimensional region of $\mathbb{R}^n$ and contains the elements x_j, $1 \leqslant j \leqslant n$, and the solution domain is $\Omega \subset \mathbb{R}^n \times (t_0, t)$. The elements of $q(\mathbf{x}, t)$ are the dependent variables, and $\mathbf{f}(q)$ is the flux vector. For the CFD problem class of interest, the Euler equations have the definitions

$$q \equiv \begin{Bmatrix} \rho \\ \rho u_i \\ \rho e \end{Bmatrix}, \qquad \mathbf{f} \equiv \begin{Bmatrix} \rho u_j \\ u_j \rho u_i + p\delta_{ij} \\ u_j(\rho e + p) \end{Bmatrix}, \tag{2}$$

where ρ is density, ρu_i is the momentum vector, ρe is total internal energy, p is pressure and δ_{ij} is the Kronecker delta. For a polytropic perfect gas, the equation of state is $p = (\gamma - 1)[\rho e - (1/2)\rho u_j u_j]$.

For the Euler equations, $\mathbf{f}$ is a homogeneous function of degree one in q with a similarity transformation that simultaneously diagonalizes the flux vector Jacobian matrix $\mathbf{A}$, i.e.

$$\mathbf{f}_\mathbf{x} = \frac{\partial f_j}{\partial x_j} = A_j \frac{\partial q}{\partial x_j} = [\mathbf{A}] q_\mathbf{x} = [S][\Lambda][S]^{-1} q_\mathbf{x}. \tag{3}$$

In one dimension, for example, $j = 1$ and the elements of the diagonal matrix $[\Lambda]$ are $\lambda_1 = \{u_1, u_1 + a_0, u_1 - a_0\}$, where a_0 is the sound speed. The multidimensional definitions for $[\Lambda]$ have been reported by Hughes and Tezduyar.[11]

The Taylor weak-statement

The construction of a finite element weak-statement discrete approximate solution to equation (1) involves identification of a finite dimensional subspace $S^h \subset H^1$ from which the trial functions for $q^h(\mathbf{x}, t)$ may be extracted, and a subspace $V^h \subset H_0^1$ for the test functions $v^h(\mathbf{x})$, which are arbitrary. The direct extension of finite element methods developed for elliptic boundary value problems defines q^h and v^h to be identical, yielding the so called (Bubnov–)Galerkin weak statement

$$\int_\Omega v^h L(q^h) \equiv 0, \quad \text{for all} \quad v^h \in V^h. \tag{4}$$

For an unsteady problem, the usual assumption for $q^h(\cdot)$ is that space and time are separable; hence equation (4) yields an ordinary differential equation system written on the time-derivatives of

$q^h(\mathbf{x}, t)$ at the nodes $\{\mathbf{X}\}$ of the discretization $\cup\Omega_h \subset \mathbb{R}^n$. Thus, the Galerkin weak statement, equation (4), provides the data needed to evaluate a discrete Taylor series for expressing the temporal evolution of the nodal variable array $\{Q(t)\}$.

The cited family of Petrov–Galerkin CFD algorithms, developed to embed stability mechanisms for convection-dominated flows, are principally distinguished by alternative definitions for the weak-statement test space $v^h(\mathbf{x})$. In direct distinction, the Taylor weak statement developed herein as a generalization of the development of Donea,[9] interchanges the formulational order of the weak statement and Taylor series and then employs identical trial and test spaces. Since equation (1) defines an evolutionary process, there must exist the Taylor series

$$q^{n+1} = q^n + \Delta t\, q_t^n + (1/2)\Delta t^2 q_{tt}^n + \tfrac{1}{6}\Delta t^3 q_{ttt}^n + \cdots, \tag{5}$$

where the subscripts t denote the order of temporal derivative at t_n, and $t_{n+1} = t_n + \Delta t$.

Equation (1) allows restatement of the temporal derivatives in equation (5), using equation (3). The first term is

$$q_t = -\mathbf{f}_x = -\mathbf{f}_q q_x \equiv -\mathbf{A} q_x = -A_j \frac{\partial q}{\partial x_j}, \tag{6}$$

where $\mathbf{A}$ is the Jacobian of the flux vector $\mathbf{f}$, with scalar components A_j, $1 \leqslant j \leqslant n$, and the last form in equation (6) employs the repeated index tensor summation convention for clarity. The second term in equation (3) becomes

$$q_{tt} = -\left(\frac{\partial f_j}{\partial x_j}\right)_t = -\frac{\partial}{\partial x_j}\left(\frac{\partial f_j}{\partial t}\right) = -\frac{\partial}{\partial x_j}\left(\frac{\partial f_j}{\partial q} q_t\right) = \frac{\partial}{\partial x_j}\left(\frac{\partial f_j}{\partial q}\frac{\partial f_k}{\partial x_k}\right) = \frac{\partial}{\partial x_j}\left(A_j A_k \frac{\partial q}{\partial x_k}\right).$$

Hence, q_{tt} is eligible for replacement using a linear combination of the last two forms; thus, for $-\bar{\alpha} + \bar{\beta} = 1$,

$$q_{tt} \equiv \frac{\partial}{\partial x_j}\left[\bar{\alpha} A_j q_t + \bar{\beta} A_j A_k \frac{\partial q}{\partial x_k}\right]. \tag{7}$$

Proceeding through similar arguments, the third derivative is expressible as the linear combination

$$q_{ttt} = \cdots \equiv \frac{\partial}{\partial x_j}\left\{\bar{\gamma}\left[A_j A_k \frac{\partial}{\partial x_k} + \frac{\partial}{\partial x_k}(A_j A_k)\right] q_t + \bar{\mu}\left[A_j A_k \frac{\partial}{\partial x_k} + \frac{\partial}{\partial x_k}(A_j A_k)\right] A_l \frac{\partial q}{\partial x_l}\right\}. \tag{8}$$

The coefficients $\bar{\alpha}$, $\bar{\beta}$ and $\bar{\gamma}$, $\bar{\mu}$ form convex sums; their definition ultimately reflects choices in the specific algorithm final functional form. For example, Donea[9] defines $\bar{\alpha} \equiv 0 \equiv \bar{\mu}$ for the original Taylor–Galerkin algorithm. Inserting equations (6)–(8) into equation (5), and collecting terms yields

$$\begin{aligned}\frac{q^{n+1} - q^n}{\Delta t} = &-\frac{\partial f_j^n}{\partial x_j} + \frac{\Delta t}{2}\frac{\partial}{\partial x_j}\left(\bar{\alpha} A_j q_t + \bar{\beta} A_j \frac{\partial f_k}{\partial x_k}\right)^n + \frac{\Delta t^2}{6}\frac{\partial}{\partial x_j}\left\{\bar{\gamma}\left[A_j A_k \frac{\partial}{\partial x_k} + \frac{\partial}{\partial x_k}(A_j A_k)\right] q_t \right.\\ &\left. + \bar{\mu}\left[A_j A_k \frac{\partial}{\partial x_k} + \frac{\partial}{\partial x_k}(A_j A_k)\right]\frac{\partial f_l}{\partial x_l}\right\}^n.\end{aligned} \tag{9}$$

The left side of equation (9) expresses the discrete approximation to q_t. Proceeding to the limit as $\Delta t \to 0$, but retaining the two higher-order terms yields the (non-discrete) modified conservation law statement as

$$L_t(q) \equiv q_t - \frac{\Delta t}{2}\frac{\partial}{\partial x_j}\left[\bar{\alpha} A_j q_t + \frac{\bar{\gamma}\Delta t}{3}\frac{\partial}{\partial x_k}(A_j A_k q_t)\right]$$

$$+\frac{\partial f_j}{\partial x_j}-\frac{\Delta t}{2}\frac{\partial}{\partial x_j}\left[\bar{\beta}A_j\frac{\partial f_k}{\partial x_k}+\frac{\bar{\mu}\Delta t}{3}\frac{\partial}{\partial x_k}\left(A_jA_k\frac{\partial f_l}{\partial x_l}\right)\right]+\cdots=0. \tag{10}$$

Equation (10) is the conservation law form desired for construction of the Taylor weak statement, wherein Δt does not vanish. It is interesting to note that equation (10) can be satisfied identically by the exact solution to equation (1) by relaxing the convex constraints so that $\bar{\alpha}=\bar{\beta}$ and $\bar{\gamma}=\bar{\mu}$. Of course, equation (9) no longer represents an exact Taylor series, but we will verify that this choice constitutes a published algorithm. Finally, equation (10) can also be written in a form devoid of **f** as

$$\begin{aligned}L_w(q)\equiv q_t+A_j\frac{\partial q}{\partial x_j}-\Delta t\frac{\partial}{\partial x_j}[\alpha A_jq_t]-\Delta t^2\frac{\partial}{\partial x_j}\left[\gamma A_j\frac{\partial}{\partial x_k}(A_kq_t)\right]\\-\Delta t\frac{\partial}{\partial x_j}\left[\beta A_jA_k\frac{\partial q}{\partial x_k}\right]-\Delta t^2\frac{\partial}{\partial x_j}\left[\mu A_j\frac{\partial}{\partial x_k}\left(A_kA_l\frac{\partial q}{\partial x_l}\right)\right]+\cdots,\end{aligned} \tag{11}$$

for the definitions

$$\begin{aligned}\alpha&\equiv\frac{\bar{\alpha}}{2}+\frac{\bar{\gamma}\Delta t}{6}\frac{\partial A_k}{\partial x_k},\\ \beta&\equiv\frac{\bar{\beta}}{2}+\frac{\bar{\mu}\Delta t}{6}\frac{\partial A_l}{\partial x_l},\\ \gamma&\equiv\frac{\bar{\gamma}}{6},\\ \mu&\equiv\frac{\bar{\mu}}{6},\end{aligned} \tag{12}$$

where $\bar{\alpha},\bar{\beta},\bar{\gamma}$ and $\bar{\mu}$ remain specificable through the original definitions.

Constructing the weak statement for the Taylor series (11) follows the standard finite element procedures. From $S^h\subset H^m$, $m\geqslant 1$, select the elements $\Psi_j(\mathbf{x})\in S^h$ to construct the approximation $q^h(\mathbf{x},t)$ as

$$q(\mathbf{x},t)\approx q^h(\mathbf{x},t)\equiv\sum_j Q_j(t)\Psi_j(\mathbf{x}). \tag{13}$$

Similarly, from the subspace $V^h\subset H^m$ establish the test function approximation,

$$v(\mathbf{x})\approx v^h(\mathbf{x})\equiv\sum_j V_j\Psi_j(\mathbf{x}). \tag{14}$$

Then form the (Galerkin) finite element approximation to the weak statement, equation (4), for the Taylor series (11), as

$$\int_\Omega v^h(\mathbf{x})L_w(q^h)\,d\mathbf{x}\equiv 0,\quad\text{for all}\quad v^h\in V^h. \tag{15}$$

Substituting equation (11), projecting the exterior **x** derivatives onto v^h, accounting for arbitrary V_j and denoting a column matrix as $\{\ \}$ produces the 'Taylor weak statement':

$$\begin{aligned}L_w(\{Q\})\equiv&\int_\Omega\{\Psi\}\left(q_t^h+A_j^h\frac{\partial q^h}{\partial x_j}\right)d\mathbf{x}\\&+\Delta t\int_\Omega\frac{\partial\Psi}{\partial x_j}A_j^h\left(\alpha q_t^h+\beta A_k^h\frac{\partial q^h}{\partial x_k}\right)d\mathbf{x}\end{aligned}$$

$$+\Delta t^2\int_\Omega \frac{\partial \Psi}{\partial x_j}A_j^h\frac{\partial}{\partial x_k}\left(\gamma A_k^h q_t^h+\mu A_k^h A_l^h\frac{\partial q^h}{\partial x_l}\right)\mathrm{d}\mathbf{x}$$

$$-\Delta t\oint_{\partial\Omega}\{\Psi\}A_j^h\left(\alpha q_t^h+\beta A_k^h\frac{\partial q^h}{\partial x_k}\right)\cdot\hat{n}_j\,\mathrm{d}\boldsymbol{\sigma}$$

$$-\Delta t^2\oint_{\partial\Omega}\{\Psi\}A_j^h\frac{\partial}{\partial x_k}\left(\gamma A_k^h q_t^h+\mu A_k^h A_l^h\frac{\partial q^h}{\partial x_l}\right)\cdot\hat{n}_j\,\mathrm{d}\boldsymbol{\sigma}\equiv\{0\}. \tag{16}$$

Linear algebra statement

Any suitable selection for $\Psi_j(\mathbf{x})$ permits evaluation of the integrals in equation (16). Through the appearance of q_t^h equation (16) is a first-order ordinary differential equation system written on the expansion coefficient set $\{Q\}$, defined in equation (13), of the form

$$[M_1(\ \ )]\frac{d\{Q\}}{dt}+[M_2(\ \ )]\{Q\}+\{b\}=\{0\}. \tag{17}$$

The square matrices $M_1(\ \ )$ and $M_2(\ \ )$ are functions of $\alpha,\ldots,\mu,\Delta t$ and $\mathbf{A}^h$, as formed for the specific $\Psi_j(\mathbf{x})$ definition and $\{b\}$ contains any data. The evolution of $\{Q\}$ is determined using a discrete Taylor series; for example, the family of simple one-step procedures is

$$\{Q\}^{n+1}\equiv\{Q\}^n+\Delta t\left(\theta\frac{\mathrm{d}\{Q\}^{n+1}}{\mathrm{d}t}+(1-\theta)\frac{\mathrm{d}\{Q\}^n}{\mathrm{d}t}\right), \tag{18}$$

where $0\leqslant\theta\leqslant 1$ is the parameter defining the implicitness of the derivative evaluation. Substituting equation (17) for the derivatives in equation (18), and clearing through produces the Taylor weak statement algorithm linear algebra statement

$$\{F\}=[M_1](\{Q\}^{n+1}-\{Q\}^n)+\Delta t\theta([M_2(\ \ )]\{Q\}+\{b\})^{n+1}$$
$$+\Delta t(1-\theta)([M_2(\ \ )]\{Q\}+\{b\})^n. \tag{19}$$

The Newton iterative solution algorithm for equation (19) is

$$[J]_p^{n+1}\{\delta Q\}_{p+1}^{n+1}=-\{F\}_p^{n+1}, \tag{20}$$

where p is the iteration index, $\{\delta Q\}_{p+1}\equiv\{Q\}_{p+1}-\{Q\}_p$ and the Newton Jacobian is defined as

$$[J]^{n+1}\equiv\frac{\partial\{F\}^{n+1}}{\partial\{Q\}^{n+1}}. \tag{21}$$

THEORETICAL ANALYSIS

Linear trial space implementation

The Taylor weak statement, equation (16), and the terminal linear algebra statement, equation (19), contain arbitrariness regarding the definition of the trial space $\Psi_j(\mathbf{x})$, the parameters α, β, γ, μ and Δt through the Taylor series conservation law restatement, and the integration algorithm implicitness parameter θ. Therefore, a theoretical analysis is required to establish appropriate values of these data upon definition of suitable norms. The developed procedure is a Fourier analysis of the fully discrete statement, equation (19), for the simplest definition of $\Psi_j(\mathbf{x})$ in one dimension for a linearized, scalar equation. Thus, for this analysis, equation (1) takes the form

$$q_t + \mathbf{f}_x \equiv q_t + aq_x = 0 \tag{22}$$

hence $A_j = A_1 \equiv a$ in equation (16). For, equation (13), the simplest trial space is the union of piecewise linear monomials. Expressed in terms of the linear cardinal basis $\{N_1(\zeta)\}$,

$$q(x,t) \approx q^h(x,t) = \sum_j Q_j(t)\Psi_j(x) = \bigcup_e \{N_1(\zeta)\}^{\mathrm{T}}\{Q(t)\}_e \tag{23}$$

for any discretization of $\Omega \subset R^1$. For reference,

$$\{N_1(\zeta)\} = \begin{Bmatrix}\zeta_1\\ \zeta_2\end{Bmatrix} = \begin{Bmatrix}1-\bar{x}/h_e\\ \bar{x}/h_e\end{Bmatrix}, \tag{24}$$

where h_e is the element measure and $\bar{x}$ is a local Cartesian co-ordinate.

For these restrictions, the Taylor weak statement, equation (16), takes the specific form

$$\begin{aligned} L_w(\{Q\}) = S_e\Big[&\int_{\Omega_e} \{N\}(\{N\}^{\mathrm{T}}\{Q\}'_e + a\{N\}_x^{\mathrm{T}}\{Q\}_e)\,\mathrm{d}x \\ &+ \Delta t \int_{\Omega_e} a\{N\}_x(\alpha\{N\}^{\mathrm{T}}\{Q\}'_e + \beta a\{N\}_x^{\mathrm{T}}\{Q\}_e)\,\mathrm{d}x \\ &+ \Delta t^2 \int_{\Omega_e} a\{N\}_x(\gamma a\{N\}^{\mathrm{T}}\{Q\}'_e + \mu a^2\{N\}_x^{\mathrm{T}}\{Q\}_e)_x\,\mathrm{d}x\Big]. \end{aligned} \tag{25}$$

In equation (25), the assembly operator S_e signifies the familiar row-wise matrix addition projecting element data into the global matrix statement, $\{Q\}'_e \equiv \mathrm{d}\{Q\}_e/\mathrm{d}t$, and the surface integrals in equation (16) are assumed to assemble to zero contributions. For the scalar flux vector Jacobian (a) assumed constant, all but the last term in equation (25) can be directly evaluated using $\{N_1\}$. Hence, define the generic element matrices

$$\begin{aligned} M_e &\equiv \int_{\Omega_e} \{N\}\{N\}^{\mathrm{T}}\mathrm{d}x = \frac{h_e}{6}\begin{bmatrix}2 & 1\\ 1 & 2\end{bmatrix}, \\ C_e^{\mathrm{T}} &\equiv h_e \int_{\Omega_e} \{N\}_x\{N\}^{\mathrm{T}}\mathrm{d}x = \frac{h_e}{2}\begin{bmatrix}-1 & 1\\ -1 & 1\end{bmatrix}, \\ C_e &\equiv h_e \int_{\Omega_e} \{N\}\{N\}_x^{\mathrm{T}}\mathrm{d}x = \frac{h_e}{2}\begin{bmatrix}-1 & -1\\ 1 & 1\end{bmatrix}, \\ D_e &\equiv h_e^2 \int_{\Omega_e} \{N\}_x\{N\}_x^{\mathrm{T}}\mathrm{d}x = h_e\begin{bmatrix}1 & -1\\ -1 & 1\end{bmatrix}, \end{aligned} \tag{26}$$

with the conventional names 'mass matrix' (M_e), 'convection matrix' (C_e) and its transpose (C_e^{T}), and 'diffusion matrix' (D_e).

The last term in equation (25) involves too many derivatives to be supported by test and trial spaces constructed using $\{N_1\}$. Increasing the test space degree to quadratic, an additional integration by parts can be performed yielding an evaluable expression. Alternatively, the new elemental dependent variable $\{\Delta Q\}_e$ can be defined to account for one x-derivative. Both procedures yield the same 'upwind' element formula (see Appendix I) upon assembly over a sufficient number of adjacent elements of uniform measure $h_e = h$. The resultant form prompts the definition

$$S_e(E_e) \equiv S_e\left(h_e^3 \int_{\Omega_e} \{N\}_x \{N\}_{xx}^{\mathrm{T}} \mathrm{d}x\right) = \begin{cases} h \begin{bmatrix} 1 & -1 & 0 \\ -2 & 2 & 0 \\ 1 & -1 & 0 \end{bmatrix}, & a > 0, \\ h \begin{bmatrix} 0 & 1 & -1 \\ 0 & -2 & 2 \\ 0 & 1 & -1 \end{bmatrix}, & a < 0. \end{cases} \tag{27}$$

Using equations (26) and (27), the linear basis Taylor weak statement (equation (25)) takes the specific form

$$L_{\mathrm{w}}(\{Q\}) = S_e\left\{\left[M_e + \alpha\left(\frac{a\Delta t}{h}\right)_e C_e^{\mathrm{T}} + \gamma\left(\frac{a\Delta t}{h}\right)_e^2 D_e\right]\frac{\mathrm{d}\{Q\}}{\mathrm{d}t} + \left(\frac{a}{h}\right)_e\left[C_e + \beta\left(\frac{a\Delta t}{h}\right)_e D_e + \mu\left(\frac{a\Delta t}{h}\right)_e^2 E_e\right]\{Q\}_e\right\}. \tag{28}$$

The Fourier analysis is facilitated by assembling each term in equation (28) over the generic pair of finite element domains sharing the common node x_j. It is easy to show that, for a uniform discretization,

$$\begin{aligned} &S_e(M_e) \to h\left(1 + \frac{\delta^2}{6}\right), \\ &S_e(C_e) \to h\Delta_0, \\ &S_e(C_e^{\mathrm{T}}) \to -h\Delta_0, \\ &S_e(D_e) \to -h\delta^2, \\ &S_e(E_e) \to \begin{cases} h\delta^2\Delta_-, & a > 0, \\ h\delta^2\Delta_+, & a < 0, \end{cases} \end{aligned} \tag{29}$$

where Δ_0, δ^2 and $\delta^2\Delta_{\mp}$ are the second-order finite difference equivalents of first and second and the upwind third spatial derivatives. In terms of these operators, and for the Courant number definition $c \equiv a\Delta t/h$, equation (28) can be written in the finite difference recursion relation form

$$L_{\mathrm{w}}(Q_j) = [1 - \alpha c\Delta_0 + (\tfrac{1}{6} - \gamma c^2)\delta^2]\frac{\mathrm{d}Q_j}{\mathrm{d}t} + \frac{c}{\Delta t}[\Delta_0 - \beta c\delta^2 + \mu c^2\delta^2\Delta_{\mp}]Q_j = 0. \tag{30}$$

Equation (30) provides the specific restricted form of equation (17) for the analysis. Substituting into equations (18) and (19), and writing equation (20) in the linearized non-iterative form yields the TWS algorithm linear algebra statement expressed in the finite difference form

$$[1 + \alpha_{\mathrm{A}}\Delta_0 + (\tfrac{1}{6} - \alpha_{\mathrm{B}})\delta^2 + \alpha_{\mathrm{C}}\delta^2\Delta_{\mp}]\,\Delta Q_j^{n+1} = -c[\Delta_0 - \alpha_{\mathrm{D}}\delta^2 + \alpha_{\mathrm{E}}\delta^2\Delta_{\mp}]\,Q_j^n. \tag{31}$$

For equation (31), $\Delta Q_j^{n+1} \equiv Q_j^{n+1} - Q_j^n$, and in terms of the original Taylor series parameters (equations (7) and (8))

$$\begin{aligned} \alpha_{\mathrm{A}} &\equiv c[\theta - (\bar{\alpha}/2) - \bar{\gamma}(\Delta t a_x/3)], \\ \alpha_{\mathrm{B}} &\equiv -c^2[(\bar{\gamma}/6) + \theta\{(\bar{\beta}/2) + \bar{\mu}(\Delta t a_x/3)\}], \\ \alpha_{\mathrm{C}} &\equiv \theta c^3\bar{\mu}/6, \\ \alpha_{\mathrm{D}} &\equiv c[(\bar{\beta}/2) + \bar{\mu}(\Delta t a_x/3)], \end{aligned}$$

$$\alpha_E \equiv c^2\bar{\mu}/6,$$
$$c \equiv a\Delta t/\Delta x. \tag{32}$$

Fourier stability analysis

The Fourier series representation of the analytical solution $q(x,t)$ to equation (22) is

$$q(x,t) = \sum_{j=-\infty}^{\infty} Q_j e^{i(\omega_j x + \alpha_j t)}, \tag{33}$$

where $\omega_j = 2\pi/\lambda_j$ is the wave number of the jth component of wavelength λ_j, α_j is the temporal frequency and $i \equiv \sqrt{-1}$. By virtue of the linearity assumption, the analysis can focus on only the jth Fourier mode q_j. Substituting the corresponding expression into equation (22) yields $\alpha_j = -a\omega_j$. Hence, the typical Fourier term of the exact solution to equation (22) can be written as

$$q(x,t) = Qe^{i\omega(x-at)}. \tag{34}$$

Assuming that the discrete approximate solution $q^h(x,t)$ behaves in a similar manner, for the typical mode assume

$$q^h(j\Delta x,t) = Qe^{i\omega(j\Delta x - \bar{\gamma}t)}, \tag{35}$$

where $\bar{\gamma} \equiv \bar{\beta} + i\bar{\delta}$, and $\bar{\beta}$ and $\bar{\delta}$ are real functions. Substituting this definition, and multiplying by $e^{-i\omega at}$ produces

$$q^h(j\Delta x,t) = Qe^{\omega t[\bar{\delta} + i(a-\bar{\beta})]}e^{i\omega(j\Delta x - at)}. \tag{36}$$

Hence, the functional form for the semi-discrete phase error e^h at $x = j\Delta x$ is $e^h = \omega(a-\bar{\beta})t$, and the artificial dissipation mechanism is embedded in $\bar{\delta}$.

After an elapse of time increment Δt, the discrete approximate solution Fourier mode is

$$\begin{aligned} q_\Delta(j\Delta x, t+\Delta t) &\equiv Qe^{i\omega[j\Delta x - \bar{\gamma}(t+\Delta t)]} \\ &\equiv e^{-i\omega\bar{\gamma}\Delta t}Qe^{i\omega(j\Delta x - \bar{\gamma}t)} \\ &\equiv gq^h(j\Delta x,t). \end{aligned} \tag{37}$$

Thus, the discrete solution Fourier mode amplification factor g is

$$\begin{aligned} g &\equiv e^{-i\omega\bar{\gamma}\Delta t} = e^{-i\omega(\bar{\beta}+i\bar{\delta})\Delta t} \\ &= e^{\omega\bar{\delta}\Delta t}[\cos(\omega\bar{\beta}\Delta t) - i\sin(\omega\bar{\beta}\Delta t)]. \end{aligned} \tag{38}$$

From equation (38), the phase speed Φ of a Fourier mode, after an elapse of one time interval Δt, is

$$\Phi \equiv \tan^{-1}\left(\frac{\mathrm{Im}(g)}{\mathrm{Re}(g)}\right) = -\omega\bar{\beta}\Delta t. \tag{39}$$

Further, the discrete solution phase error is defined as $e_\Delta = \omega\Delta t(a-\bar{\beta})$.

Therefore, algorithm stability and dissipation/dispersion error mechanisms are characterized by the solution for $\bar{\gamma} = \bar{\beta} + i\bar{\delta}$. From equation (37), $q_\Delta^{n+1} - q_\Delta^n = (g-1)g_\Delta^n$; hence, using equation (31),

$$g - 1 = \frac{-c[\Delta_0 - \alpha_D\delta^2 + \alpha_E\delta^2\Delta_\mp]e^{i\omega(j\Delta x)}}{\left[1 + \alpha_A\Delta_0 + \left(\frac{1}{6} - \alpha_B\right)\delta^2 + \alpha_C\delta^2\Delta_\mp\right]e^{i\omega(j\Delta x)}}. \tag{40}$$

Noting the following identities (for $m \equiv \omega\Delta x$):

$$\begin{aligned}
\Delta_0 e^{i\omega(j\Delta x)} &= i(\sin m)e^{i\omega(j\Delta x)},\\
\delta^2 e^{i\omega(j\Delta x)} &= 2(\cos m - 1)e^{i\omega(j\Delta x)},\\
\delta^2\Delta_{\mp} e^{i\omega(j\Delta x)} &= 2(\cos m - 1)[\mp(\cos m - 1) + i(\sin m)]e^{i\omega(j\Delta x)},
\end{aligned} \tag{41}$$

equation (40) takes the form

$$g - 1 = \frac{c([2\alpha_D(\cos m - 1) + 2(\operatorname{sgn} a)\alpha_E(\cos m - 1)^3] - i(\sin m)[1 + 2\alpha_E(\cos m - 1)])}{[1 + (\frac{1}{3} - 2\alpha_B)(\cos m - 1) - 2(\operatorname{sgn} a)\alpha_c(\cos m - 1)^2] + i(\sin m)[\alpha_A + 2\alpha_c(\cos m - 1)]}, \tag{42}$$

where $(\operatorname{sgn} a)$ is the sign of the flux vector Jacobian a.

Expanding the terms in equation (42) in a Taylor series in m (see Appendix II) the solution for the fully discrete solution amplification factor g is

$$\begin{aligned}
g = 1 &+ c[-\alpha_1 m^2 + (\beta_1 - \beta_0\alpha_1)m^4 - ((\gamma_1 - \gamma_0\alpha_1) - \beta_0(\beta_1 - \beta_0\alpha_1))m^6 + O(m^8)]\\
&- ic[m - (\beta_2 - \beta_0)m^3 + ((\gamma_2 - \gamma_0) - \beta_0(\beta_2 - \beta_0))m^5\\
&- ((\mu_2 - \mu_0) - \gamma_0(\beta_2 - \beta_0) - \beta_0(\gamma_2 - \gamma_0) + \beta_0^2(\beta_2 - \beta_0))m^7 + O(m^9)].
\end{aligned} \tag{43}$$

The coefficients $\alpha_0, \alpha_1, \beta_0, \ldots, \mu_2$ in equation (43) are related to the parameters $\alpha_A, \ldots, \alpha_E$ (hence, $\bar{\alpha}, \bar{\beta}, \bar{\gamma}, \bar{\mu}, \theta$) of the Taylor weak statement as

$$\begin{aligned}
\alpha_1 &= \alpha_A + \alpha_D,\\
\beta_1 &= \tfrac{1}{3}\alpha_A + \tfrac{1}{4}\alpha_D + \alpha_C + \tfrac{1}{2}(\operatorname{sgn} a)\alpha_E - \alpha_B\alpha_D + \alpha_A\alpha_E,\\
\gamma_1 &= \tfrac{16}{360}\alpha_A + \tfrac{5}{12}\alpha_C + \tfrac{11}{360}\alpha_D + \tfrac{1}{6}(\operatorname{sgn} a)\alpha_E + \tfrac{5}{12}\alpha_A\alpha_E\\
&\quad - \tfrac{1}{6}\alpha_B\alpha_D - \tfrac{1}{2}(\operatorname{sgn} a)(\alpha_B\alpha_E + \alpha_C\alpha_D) + \alpha_C\alpha_E,
\end{aligned} \tag{44a}$$

$$\begin{aligned}
\beta_2 &= \alpha_A\alpha_D - \alpha_B + \alpha_E + \tfrac{1}{3},\\
\gamma_2 &= \tfrac{1}{4}\alpha_A\alpha_D + \tfrac{1}{2}(\operatorname{sgn} a)\alpha_A\alpha_E - \alpha_B\alpha_E + \alpha_C\alpha_D\\
&\quad - \tfrac{1}{4}\alpha_B + \tfrac{5}{12}\alpha_E - \tfrac{1}{2}(\operatorname{sgn} a)\alpha_C + \tfrac{1}{20},\\
\mu_2 &= \tfrac{11}{2520} + \tfrac{1}{40}\alpha_A\alpha_D + \tfrac{1}{6}(\operatorname{sgn} a)\alpha_A\alpha_E - \tfrac{1}{3}\alpha_B\alpha_E + \tfrac{1}{3}\alpha_C\alpha_D\\
&\quad - \tfrac{1}{40}\alpha_B - \tfrac{1}{6}(\operatorname{sgn} a)\alpha_C + \tfrac{1}{12}\alpha_E,
\end{aligned} \tag{44b}$$

$$\begin{aligned}
\beta_0 &= -\alpha_A^2 - 2\alpha_B + \tfrac{1}{3}\\
\gamma_0 &= -\tfrac{1}{3}\alpha_A^2 - 2\alpha_A\alpha_C - (\operatorname{sgn} a)\alpha_C + \alpha_B^2 - \tfrac{1}{2}\alpha_B + \tfrac{1}{18},\\
\mu_0 &= -\tfrac{2}{45}\alpha_A^2 + \tfrac{1}{6}\alpha_B^2 - \alpha_C^2 - \tfrac{5}{6}\alpha_A\alpha_C + (\operatorname{sgn} a)\alpha_B\alpha_C\\
&\quad - \tfrac{11}{180}\alpha_B - \tfrac{1}{3}(\operatorname{sgn} a)\alpha_C + \tfrac{1}{180}.
\end{aligned} \tag{44c}$$

It appears appropriate to impose constraints on the Taylor weak statement parameters $\alpha_A, \ldots, \alpha_E$, such that the fully discrete approximate solution amplification factor $g = e^{-i\omega\gamma\Delta t}$ matches as closely as possible the analytical amplification factor $e^{-i\omega a\Delta t}$. Since

$$e^{-imc} = 1 - icm - \tfrac{1}{2}c^2m^2 + \tfrac{1}{6}ic^3m^3 + \cdots, \tag{45}$$

for equation (43) one arrives at the following definitions:

$$\begin{aligned}
\alpha_1 &\equiv \frac{c}{2},\\
\beta_2-\beta_0 &\equiv \frac{c^2}{3!},\\
\beta_1-\beta_0\alpha_1 &\equiv \frac{c^3}{4!},\\
(\gamma_2-\gamma_0)-\beta_0(\beta_2-\beta_0) &\equiv \frac{c^5}{5!},\\
(\gamma_1-\gamma_0\alpha_1)-\beta_0(\beta_1-\alpha_1) &\equiv \frac{c^6}{6!},\\
(\mu_2-\mu_0)-\gamma_0(\beta_2-\beta_0)-\beta_0(\gamma_2-\gamma_0)+\beta_0^2(\beta_2-\beta) &\equiv \frac{c^7}{7!}.
\end{aligned} \tag{46}$$

It remains to separate out the Fourier series solution expansion for the real and imaginary components of $\bar{\gamma} \equiv \bar{\beta} + i\bar{\delta}$; recall equation (35). Since $g = e^{-i\omega\bar{\gamma}\Delta t}$ then $e^{-i\omega(\bar{\gamma}-a)} = g e^{i\omega a\Delta t}$, or

$$e^{\omega\Delta t[\bar{\delta}-i(\bar{\beta}-a)]} = g e^{icm}. \tag{47}$$

From equations (45) and (46), the right side of equation (47) yields

$$\begin{aligned}
\text{RHS (47)} &= g[\cdot]\\
&= 1 + m^2\left[\frac{c^2}{2} - \alpha_1 c\right]\\
&\quad + im^3\left[\frac{c^3}{3} - \alpha_1 c^2 + (\beta_2-\beta_0)c\right]\\
&\quad + m^4\left[-\frac{c^4}{8} + \frac{\alpha_1 c^3}{2} - (\beta_2-\beta_0)c^2 + (\beta_1-\beta_0\alpha_1)c\right]\\
&\quad + im^5\left[-\frac{c^5}{30} + \frac{\alpha_1 c^4}{6} - (\beta_2-\beta_0)\frac{c^3}{2} + (\beta_1-\beta_0\alpha_1)c^2\right.\\
&\quad \left. - ((\gamma_2-\gamma_0)-\beta_0(\beta_2-\beta_0))c\right] + \cdots.
\end{aligned} \tag{48}$$

Since the left side of equation (47) is of the form

$$\text{LHS (47)} \simeq 1 + \omega(\Delta t)[\bar{\delta} - i(\bar{\beta} - a)], \tag{49}$$

equations (48) and (49) yield the required estimates of the fully discrete solution dissipation error $\omega(\Delta t)\bar{\delta}$ and phase error $\omega(\Delta t)(a-\bar{\beta})$ as

$$\omega(\Delta t)\bar{\delta} = c\left\{m^2\left[\frac{c}{2} - \alpha_1\right] + m^4\left[-\frac{c^3}{8} + \frac{\alpha_1 c^2}{2} - (\beta_2-\beta_0)c + (\beta_1-\beta_0\alpha_1)\right] + m^6(\cdot) + \cdots\right\}, \tag{50}$$

$$\omega(\Delta t)(a-\bar{\beta}) = c\left\{m^3\left[\frac{c^2}{3} - \alpha_1 c + (\beta_2-\beta_0)\right] + m^5\left[-\frac{c^4}{30} + \frac{\alpha_1 c^3}{6} - \frac{(\beta_2-\beta_0)c^2}{2} + (\beta_1-\beta_0\alpha_1)c\right.\right.$$

$$-\left((\gamma_2-\gamma_0)-\beta_0(\beta_2-\beta_0)\right)\Big]+m^7(\cdot)+\cdots\Big\}. \tag{51}$$

The leading terms in equations (50) and (51) are generally coincident with those reported in the literature as developed using local Taylor series expansions for fully discrete finite difference algorithms, e.g. donor cell, Lax–Wendroff, etc. which correspond to special cases of equation (31). The entire family of Taylor weak-statement algorithms, expressed by equation (31), has as arbitrary parameters the set of coefficients $\bar{\alpha}, \bar{\beta}, \bar{\gamma}, \bar{\mu}$ (recall equations (11) and (12)). Equation (44) defines the correlation between these parameters and θ, through $\alpha_A, \ldots, \alpha_E$ in equation (32), to the theoretical error estimates given in equations (50) and (51).

DISCUSSION AND RESULTS

The Taylor weak-statement finite element algorithm for a hyperbolic conservation law system has been derived and the linear basis implementation completed in equations (31) and (32). Choices for $\bar{\alpha}, \bar{\beta}, \bar{\gamma}, \bar{\mu}$ and θ define a specific implementation, and several families of finite difference and finite element algorithms can be established in this manner, as summarized in Table I. In this section, the associated dissipation and dispersion error solutions are characterized, from equations (50) and (51), and the performance of each algorithm is directly compared for four test cases. These elementary but definitive test cases correspond to a steady and an unsteady, one-dimensional inviscid (or viscous, as required) problem, each with a linear (a = constant) and the Burgers' non-linear ($a = q$) flux vector Jacobian. In all cases, the exact solutions are known for unequivocal comparison.

The test case solutions are graphically summarized in Figure 1 for the governing model equations

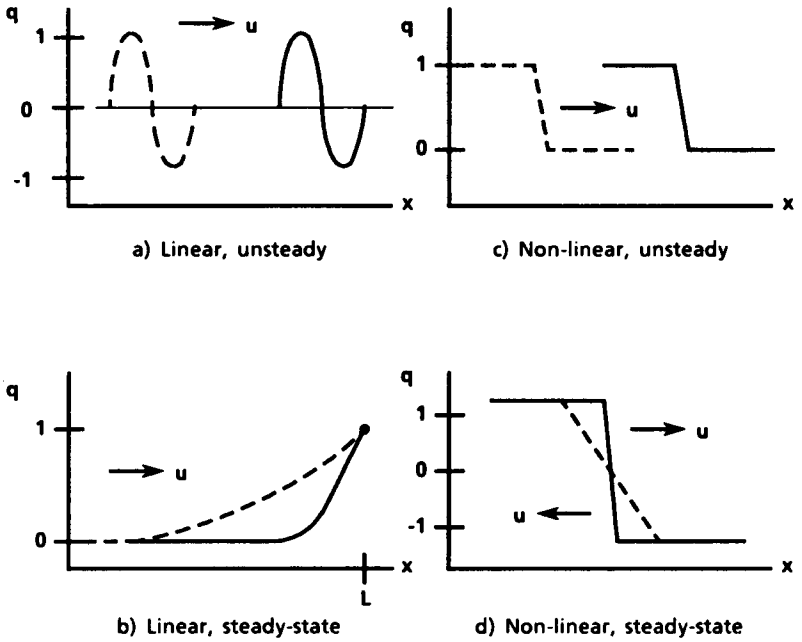

Figure 1. Model problem test cases: (---) initial condition, (———) exact solution

Table I. Summary of CFD algorithms within Taylor weak statement (equations (31) and (32))

Method	Reference	θ	α_A	$(\frac{1}{6}-\alpha_B)$	α_C	$-\alpha_D$	α_E	Comments
Taylor weak statement	This paper, equation (32)	all	$c\left(\theta-\frac{\bar{\alpha}}{2}-\frac{\bar{\gamma}}{3}-\frac{\Delta t a_x}{2}\right)$	$\frac{1}{6}-c^2\left[\frac{\bar{\gamma}}{6}+\theta\left(\frac{\bar{\beta}}{2}+\frac{\bar{\mu}}{2}-\frac{\Delta t a_x}{2}\right)\right]$	$c^3\theta\frac{\bar{\mu}}{6}$	$-c\left(\frac{\bar{\beta}}{2}+\frac{\bar{\mu}}{2}-\frac{\Delta t a_x}{2}\right)$	$c^2\frac{\bar{\mu}}{6}$	$\bar{\alpha},\bar{\beta},\bar{\gamma},\bar{\mu},\theta$ to be defined
Bubnov–Galerkin	This paper, equation (54)	all	$c\theta$	$\frac{1}{6}$	0	0	0	$\bar{\alpha}=0=\bar{\beta}=\bar{\mu}=\bar{\gamma}$
Donor-cell upwind	12	0	0	0	0	$-\frac{(\text{sgn } a)}{2}$	0	$\lvert c\rvert\leqslant 1$
Lax–Wendroff	13	0	0	0	0	$-\frac{c}{2}$	0	$\lvert c\rvert\leqslant 1$
Euler–Taylor–Galerkin	9	0	$c\bar{\theta}$	$\frac{1}{6}\frac{c^2}{6}(1-3\bar{\theta})$	0	$-c(\frac{1}{2}-\bar{\theta})$	0	$\bar{\theta}=0$ for ETG, $\bar{\theta}=\frac{1}{2}$ for CN–TG
Euler–characteristic–Galerkin	8	0	0	$\frac{1}{6}$	0	$-\frac{c}{2}$	$\frac{c^2}{6}$	$\lvert c\rvert\leqslant 1$ for this form
Swansea–Taylor–Galerkin	21	0	0	$\frac{1}{6}$	0	$-\frac{c}{2}$	0	$\lvert c\rvert\leqslant 1\sqrt{3}$ for stability
Wahlbin	1	0	$c\theta-(\text{sgn } a)$	$\frac{1}{6}-c(\text{sgn } a)\theta$	0	$-(\text{sgn } a)$	0	
Dendy	2	0	$c\theta-(\text{sgn } a)k'$	$\frac{1}{6}-c(\text{sgn } a)k'\theta$	0	$-(\text{sgn } a)k'$	0	$\text{Re}[\Phi,k\Phi_x]\leqslant C_1\lVert\Phi\rVert^2, k=k'\Delta x,$ $C_1>0$
Raymond–Garder	3	$\frac{1}{2}$	$c\theta-(\text{sgn } a)v$	$\frac{1}{6}-c(\text{sgn } a)v\theta$	0	$-(\text{sgn } a)v$	0	$v=1/\sqrt{15}$
penalty–Galerkin	7	all	$c\theta-(\text{sgn } a)v_i$	$\frac{1}{6}-c(\text{sgn } a)v_d\theta$	0	$-(\text{sgn } a)v_d$	0	$v_i,v_d\approx C_a(1/\sqrt{15}),0\leqslant C_a\leqslant 2$ for Euler equations
Hughes–Brooks SUPG	5					$-\left(\frac{a}{2}+\frac{k}{a\Delta x}\right)(\text{sgn } a)v$		steady only, $k=$ thermal conductivity
Euler–Petrov–Galerkin	6	0	0	$\frac{1}{6}-\frac{1}{6}(1-v)$	0	$-\frac{(\text{sgn } a)v}{2}$	0	$\lvert c\rvert\leqslant v\leqslant 1$
CN Petrov–Galerkin	6	$\frac{1}{2}$	$\frac{c}{2}-\frac{(\text{sgn } a)v}{2}$	$\frac{1}{6}-\frac{v}{2}\left((\text{sgn } a)\frac{c}{2}-\frac{1}{6}\right)$	0	$-\frac{(\text{sgn } a)v}{2}$	0	$\lvert c\rvert\leqslant v\leqslant 1$
Warming–Beam explicit	23	0	0	0	0	$-\frac{c}{2}$	$-\frac{(1-c)}{2}$	$\lvert c\rvert\leqslant 1, a>0$
van Leer (MUSCL)	24	1	$c\theta$	$-c(\text{sgn } a)\frac{\theta}{2}$	0	0	$-\frac{1}{2}$	Simple flux limiter ($\Phi^{\pm}\equiv 1$)
Hughes–Mallet	25	0	$\frac{l(\text{sgn } a)}{2}$	$\frac{1}{6}+\frac{1}{12}$	0	$-\frac{(\text{sgn } a)}{2}$	0	l is flux limiter, $0\leqslant l\leqslant 1$

$$q_t + aq_x = \varepsilon q_{xx} \tag{52a}$$

and

$$q_t + (\tfrac{1}{2}q^2)_x = 0, \tag{52b}$$

where ε is the viscosity coefficient. The linear unsteady case corresponds to uniform rightward propagation ($a > 0$) of a full phase sine wave, the inviscid ($\varepsilon \equiv 0$) analytical solution for which is exact preservation of the initial condition (Figure 1(a)). The steady linear test case is (must be) viscous ($\varepsilon > 0$), and is obtained numerically as the unsteady evolution from an interpolation between the end points of the analytical steady state solution to equation 52(a), which is

$$q(x) = e^{Pe[(x/L)-1]}, \tag{53}$$

where $Pe = aL/\varepsilon$ is the Peclet number. For $\varepsilon > 0$, the expressions inside the brackets for α_B and α_D (equation 32) are augmented by the 'cell Peclet number' terms $\theta\varepsilon/a\Delta x$ and $\varepsilon/a\Delta x$, respectively. The solution slope in the wall layer solution is controlled by Pe, as illustrated in Figure 1(b).

Both non-linear test cases are specified as inviscid ($\varepsilon = 0$). The unsteady case (Figure 1(c)), corresponds to a right-travelling square wave propagating into a stagnation region ($q = 0$) with (exact) solution group velocity $u = q/2$. The steady case is the intersection of two square waves with analytical solution $q = \pm 1$ at the sides of a stationary shock of strength $\Delta q = 2$ (Figure 1(d)). For both cases, the initial conditions are illustrated by dashed lines, and the exact solution is the solid line.

Bubnov–Galerkin finite element algorithm

The basic (Bubnov–) Galerkin finite element algorithm is constructed for the model differential equation (equation 52) by omitting all additional terms in the Taylor series, equation (10). Thus, $\alpha = 0 = \beta = \gamma = \mu$: hence

$$\alpha_A = c\theta$$

and

$$\alpha_B = 0 = \alpha_C = \alpha_D = \alpha_E, \tag{54a}$$

via equation (32). From equation (44), one thus obtains

$$\begin{aligned} &\alpha_1 = c\theta, \quad \beta_2 = \tfrac{1}{3}, \quad \beta_0 = -(c\theta)^2 + \tfrac{1}{3}, \\ &\beta_1 = \frac{c\theta}{3}, \quad \gamma_2 = \tfrac{1}{20}, \quad \gamma_0 = \frac{-(c\theta)^2}{3} + \frac{1}{18}, \\ &\gamma_1 = \frac{c\theta}{90}, \quad \mu_2 = \tfrac{11}{2520}, \quad \mu_0 = \frac{-2(c\theta)^2}{45} + \frac{1}{180}. \end{aligned} \tag{54b}$$

Hence, the discrete amplification factor (equation (42)) is

$$\begin{aligned} g &= 1 - \frac{ic(\sin m)}{1 + \frac{1}{3}(\cos m - 1) + ic\theta(\sin m)} \\ &= \frac{1 + \frac{1}{3}(\cos m - 1) - ic(1-\theta)(\sin m)}{1 + \frac{1}{3}(\cos m - 1) + ic\theta(\sin m)}, \end{aligned} \tag{54c}$$

and

$$\omega(\Delta t)\bar{\delta} = c\left[c(\tfrac{1}{2} - \theta)m^2 + c^3\left(-\frac{1}{8} + \frac{\theta}{2} - \theta^2 + \theta^3\right)m^4 + \cdots\right] \tag{54d}$$

$$\omega(\Delta t)(a-\bar{\beta}) = c[c^2(\tfrac{1}{3}-\theta+\theta^2)m^3+\cdots]. \tag{54e}$$

From equation (54c), $\theta = 1/2$ appears as the optimal choice, since $|g| = 1$ for all c and m. Further $[(1/2)-\theta] = 0 = [-(1/8)+(\theta/2)-\theta^2+\theta^3]$ for $\theta = 1/2$ (equation (54d)), hence the Galerkin algorithm is dissipation-free to $O(m^6)$ and the dispersion error coefficient is $c^2m^3/12$. For $\theta = 0$, equation (54d) indicates that the algorithm is unstable, since $cm^2/2 > 0$. This is of no real consequence, however, since the sign of this term changes for the stability analysis completed using the discrete solution rather than the exact solution for q^n, leading to equation (40). Conversely, for $\theta = 1$, the dominant dissipation term is $O(m^2)$; hence the Galerkin algorithm is first order accurate with large damping.

Figure 2 summarizes the Galerkin algorithm results for the four test problems. For each graph, the solid curve is the analytical solution, and the symbols are the nodal discrete approximate solutions. The short wavelength phase dispersion and relative absence of artificial dissipation are evident for the travelling wave (Figure 2(a)), for the solution computed for Courant number (non-dimensional time step) $c = 0{\cdot}8(= a\Delta t/\Delta x)$. Larger and smaller levels of Courant number aggravate and diminish, respectively, this dispersive character, as predicted by equation (54e). Definition of $\theta = 1$ introduces a large dissipation level which smooths the dispersion error (Figure 2(b)). For the steady linear problem, a Peclet number of $Pe = 40$ interpolates the non-zero portion of the exact solution over 2 cells of a 16 cell uniform mesh, and the Galerkin algorithm solution is non-monotone (Figure 2(c)). For any $Pe > 50$, the exact solution span is interpolated only over one cell. At $Pe = 180$, the $2\Delta x$ oscillation has polluted the entire solution (Figure 2(d)), and the steady-state is independent of the definition for θ.

The $\theta = 0$ and $\theta = 1/2$ Galerkin forms are basically unstable for both non-linear test problems. The order m^2 term in $\bar{\delta}$ yields the sole dissipation mechanism for $\theta > 1/2$. Figure 2(e) shows the unsteady, inviscid non-linear Burgers' result obtained using $\theta = 1$. The $2\Delta x$ oscillations behind the shock, which are primarily induced by the downstream stagnation initial condition ($q = 0$) are rather severe. Figure 2(f) confirms the oscillation reduction for the (non-stagnation) downstream initial condition $q = \frac{1}{2}$ and for $\theta = 1$. However, the choice for θ bears no impact on the non-linear, steady-state problem solution, (Figure 2(g)), the results for which firmly verify the inherent instability intrinsic to the classic Bubnov–Galerkin finite element algorithm.

Donor-cell upwind finite difference algorithm

It is convenient to reference a class of non-Bubnov–(but also non-Petrov–)Galerkin finite element algorithms to the donor-cell upwind and Lax–Wendroff finite difference algorithms. The donor cell (explicit) algorithm[12] is defined (equation (31)) by the constraints (equation (32)),

$$\begin{aligned} &\alpha_A = 0 = \alpha_C = \alpha_E = \theta, \\ &\alpha_B = \tfrac{1}{6}, \\ &\alpha_D = \frac{(\operatorname{sgn} a)}{2}, \end{aligned} \tag{55a}$$

where the definition for α_B removes the mass matrix contribution (recall equations (29)–(31)). Thus, for the Taylor weak statement, $\alpha = 0 = \gamma = \mu$ and $\beta = (\operatorname{sgn} a)/c$. In equation (44), one obtains for the Fourier analysis parameter set

$$\alpha_1 = \frac{(\operatorname{sgn} a)}{2}, \quad \beta_0 = 0, \quad \beta_2 = \tfrac{1}{6},$$

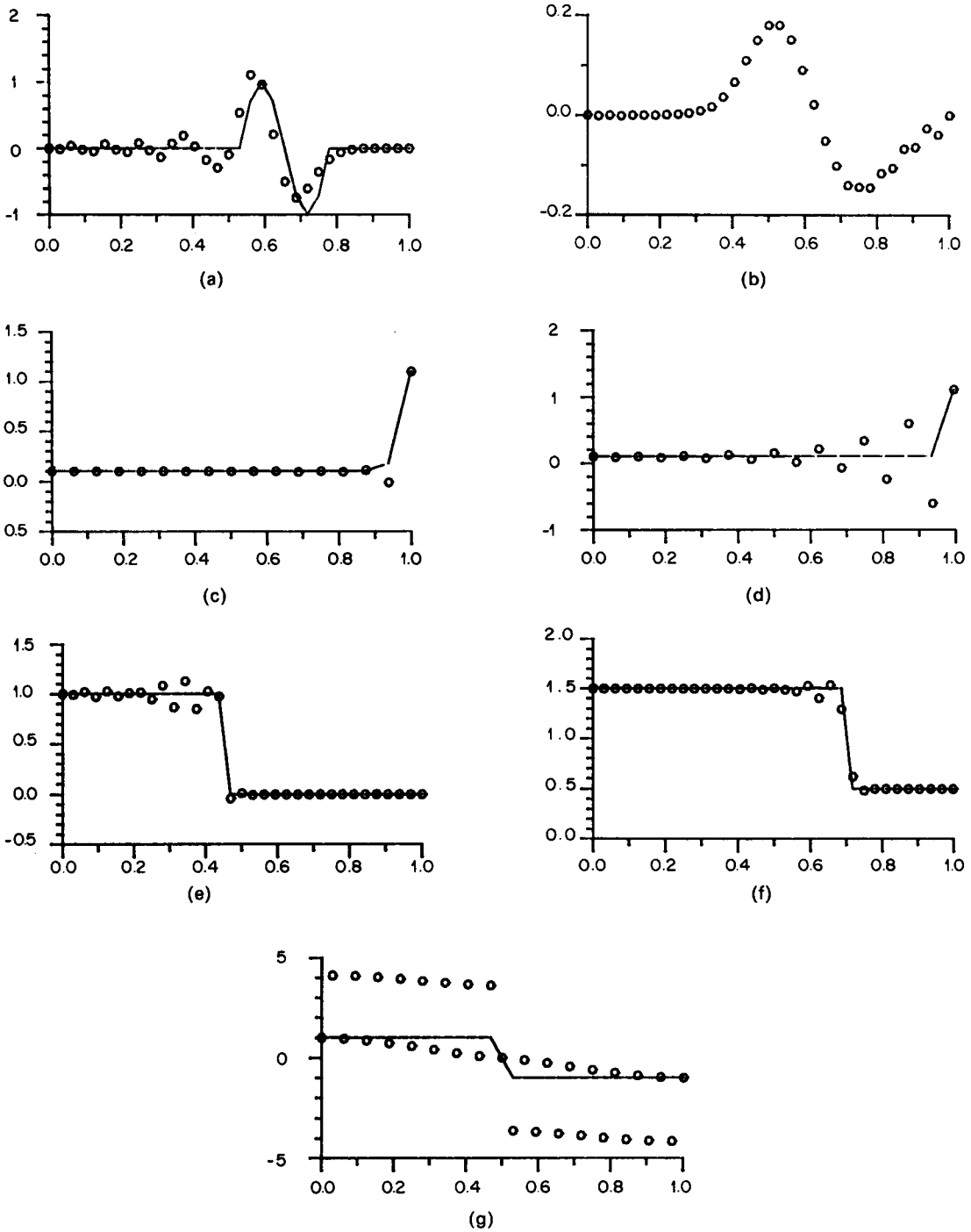

Figure 2. Bubnov–Galerkin finite element algorithm test problem solutions: (a) linear, unsteady, $\theta = 0{\cdot}5$, $c = 0{\cdot}8$; (b) linear, unsteady, $\theta = 1{\cdot}0$, $c = 0{\cdot}8$; (c) linear, steady-state, $\theta = 0{\cdot}5$, $1{\cdot}0$, $Pe = 40$; (d) linear, steady-state, $\theta = 0{\cdot}5$, $1{\cdot}0$, $Pe = 180$; (e) non-linear, unsteady $\theta = 1{\cdot}0$, $c = 0{\cdot}32$; (f) non-linear, unsteady $\theta = 1{\cdot}0$, $c = 0{\cdot}32$, no stagnation; (g) non-linear, steady-state $\theta = 0{\cdot}5$, $1{\cdot}0$

$$\beta_1 = \frac{(\operatorname{sgn} a)}{24}, \quad \gamma_0 = 0, \quad \gamma_2 = \tfrac{1}{120},$$

$$\gamma_1 = \frac{(\operatorname{sgn} a)}{720}, \quad \mu_0 = 0, \quad \omega_2 = \tfrac{1}{2(252\bar{0})}. \tag{55b}$$

The resultant Fourier solution functions (equations (43), (50) and (51)) are

$$g = 1 + c[(\cos m - 1) - \mathrm{i}(\sin m)], \tag{55c}$$

$$\omega(\Delta t)\bar{\bar{\delta}} = c[\tfrac{1}{2}(c-1)m^2 + \cdots], \tag{55d}$$

$$\omega(\Delta t)(a - \bar{\bar{\beta}}) = c[\tfrac{1}{6}(2c^2 - 3c + 1)m^3 + \cdots]. \tag{55e}$$

Since the upwind donor cell algorithm exhibits the 'unit CFL property', the optimal Courant number is unity. Stability requires $c \leqslant 1$, and for $c < 1$ the algorithm is first order accurate.

Figure 3 graphs the test case results. The unsteady linear problem solution at $c = 0{\cdot}8$ (Figure 3(a)), confirms the inherent large artificial dissipation present for any $c < 1$. The steady-state linear solution at $Pe = 40$ also confirms excess dissipation, (Figure 3(b)). The unsteady, stagnation-penetrating non-linear problem solution is not monotone at $c = 0{\cdot}32$ (Figure 3(c)), with the shock interpolated across three cells. In distinction, the solution is monotone and diffuse when a stagnation zone (point) is not present (Figure 3(d)). The non-monotone character persists for the steady state shock with nodal stagnation point (Figure 3(e)), which exhibits a quite modest one-cell over- and under-shoot.

Lax–Wendroff finite difference algorithm

The consequential difference between the donor cell and Lax–Wendroff algorithms in equation (31) is contained in α_D. Lax–Wendroff[13] is recovered by the definitions (equation (32))

$$\begin{aligned} &\alpha_A = 0 = \alpha_C = \alpha_E = \theta, \\ &\alpha_B = \tfrac{1}{6}, \\ &\alpha_D = \frac{c}{2}. \end{aligned} \tag{56a}$$

Thus, for the Taylor weak statement, $\bar{\alpha} = 0 = \bar{\gamma} = \bar{\mu}$ and $\bar{\beta} = 1$; for equation (44) we thus have

$$\alpha_1 = \frac{c}{2}, \quad \beta_0 = 0, \quad \beta_2 = \tfrac{1}{6},$$

$$\beta_1 = \frac{c}{24}, \quad \gamma_0 = 0, \quad \gamma_2 = \tfrac{1}{120}, \tag{56b}$$

$$\gamma_1 = \frac{c}{720}, \quad \mu_0 = 0, \quad \mu_2 = \tfrac{1}{2(252\bar{0})},$$

and for equations (43), (50) and (51)

$$g = 1 + c^2(\cos m - 1) - \mathrm{i}c(\sin m), \tag{56c}$$

$$\omega(\Delta t)\bar{\bar{\delta}} = c\left[\frac{c}{8}(c^2 - 1)m^4 + \cdots\right], \tag{56d}$$

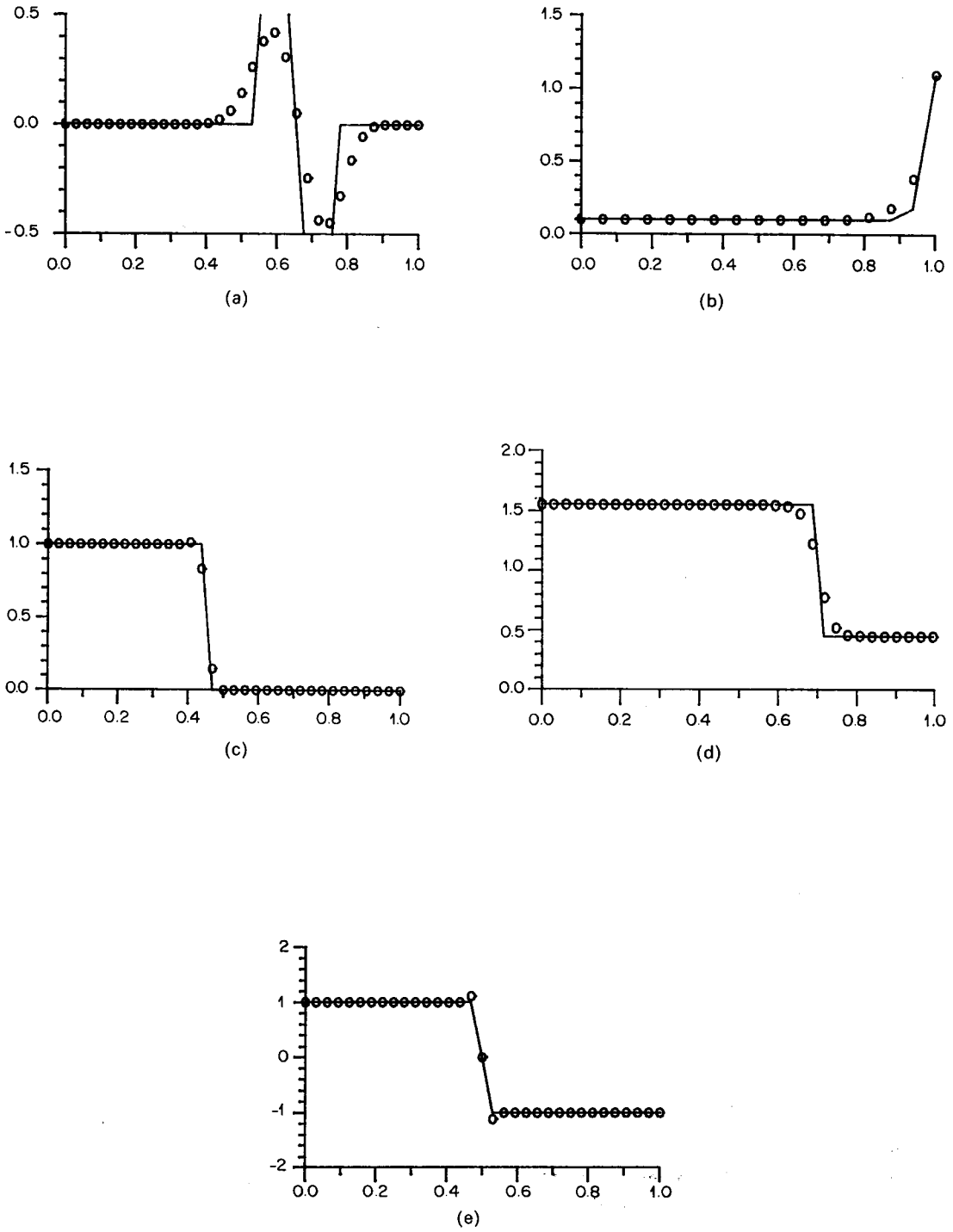

Figure 3. Donor-cell finite difference algorithm test problem solutions: (a) Linear, unsteady, $c = 0{\cdot}8$; (b) linear, steady-state, $Pe = 40$; (c) non-linear, unsteady, $c = 0{\cdot}32$; (d) non-linear, unsteady, $c = 0{\cdot}32$, no stagnation; (e) non-linear, steady-state

$$\omega(\Delta t)(a-\bar{\beta}) = c[\tfrac{1}{6}(1-c^2)m^3 + \cdots]. \tag{56e}$$

The Lax–Wendroff algorithm also exhibits the unit CFL property, and for $c < 1$ it is second-order accurate, a definite improvement over upwind donor-cell.

Figure 4 summarizes the test case results. The unsteady linear solution at $c = 0{\cdot}8$ is much superior to the donor cell results regarding artificial dissipation effects, although a significant lagging phase dispersion wake is present (Figure 4(a)). The steady linear solution at $Pe = 40$ is just distinguishable from the analytical solution (Figure 4(b)). The unsteady non-linear solution at $c = 0{\cdot}32$ is non-monotone with a pronounced lagging overshoot (Figure 4(c)). Similarly, an oscillation is generated in the steady non-linear problem solution, extending about $2\Delta x$ each side of the shock (Figure 4(d)).

Higher-order Galerkin finite element algorithms

There have recently been published three Galerkin-type finite element algorithms (in the sense that the test and trial spaces are identical, and no arbitrary coefficients are involved) that constitute select retention of higher order terms in the Taylor series conservation law restatement

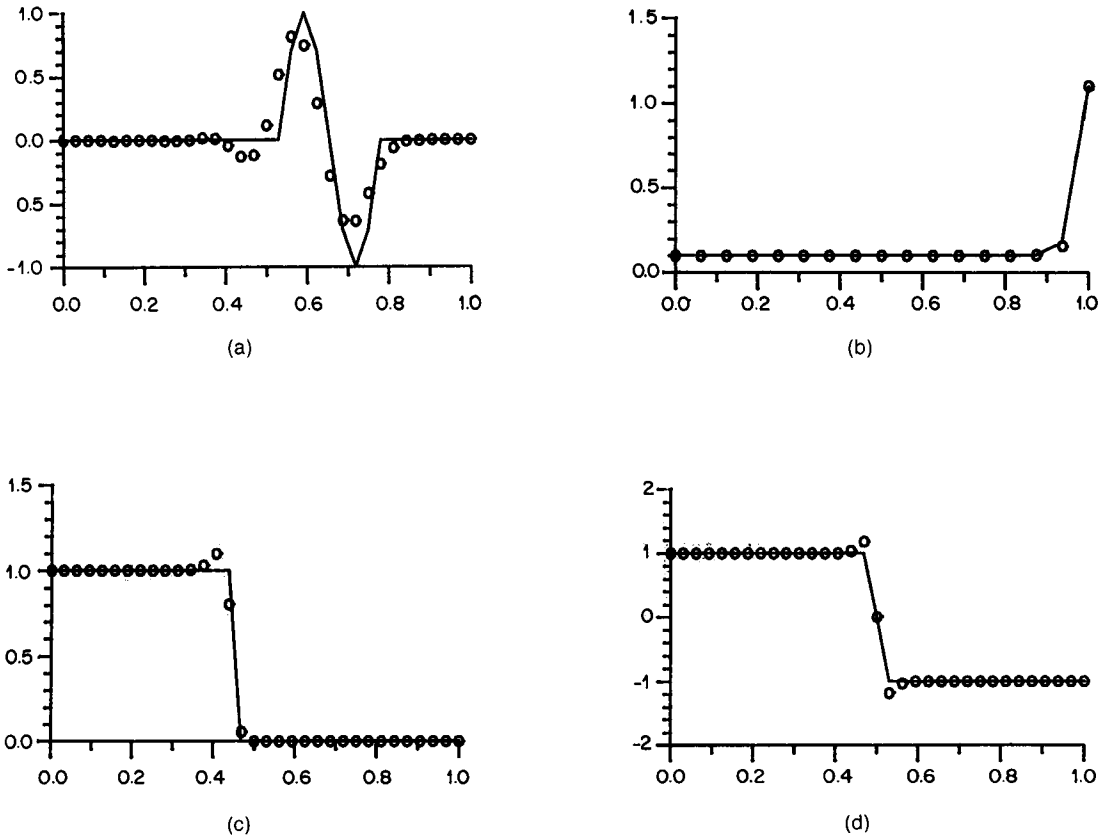

Figure 4. Lax–Wendroff finite difference algorithm test problem solutions: (a) linear, unsteady, $c = 0{\cdot}8$; (b) linear, steady-state, $Pe = 40$; (c) non-linear, unsteady, $c = 0{\cdot}32$; (d) non-linear, steady-state

(equation (11)). The Euler–Taylor–Galerkin algorithm of Donea[9,14–16] constitutes the choices $\bar{\alpha}=0=\bar{\mu}$ and $\bar{\beta}=1=\bar{\gamma}$ in equation (10), and $\theta=0$ in equation (18). Thus, for the Taylor weak-statement algorithm (equation (31)) one has the following definitions for the parameter (equation (32)):

$$\alpha_A=0=\alpha_C=\alpha_E=\theta,$$
$$\alpha_B=\frac{c^2}{6}, \tag{57a}$$
$$\alpha_D=\frac{c}{2}.$$

Conversely, the Euler–characteristic–Galerkin algorithm of Morton[8,17] stems from the definition $\bar{\alpha}=0=\bar{\gamma}$ and $\bar{\beta}=1=\bar{\mu}$ in the Taylor series (equation (10)) and $\theta=0$ in equation (18). Thus, for the constraint $|c|<1$ (due to the selected upwinding definition (equation (27)), this finite element algorithm is extracted from the Taylor weak statement (equation (31)) by the parameter definitions (equation (32))

$$\alpha_A=0=\alpha_B=\alpha_C=\theta,$$
$$\alpha_D=\frac{c}{2}, \tag{58a}$$
$$\alpha_E=\frac{c^2}{6}.$$

Note that the definitions in both equations (57a) and (58a) correspond to an exact higher order Taylor series, in distinction to the donor cell definition.

Viewing equations (57a) and (58a), one expects only subtle performance distinctions between these algorithms. Completing the algebra within equations (44), (42), (50) and (51), for the Euler–Taylor–Galerkin (ETG) algorithm one obtains

$$\alpha_1=\frac{c}{2}, \qquad \beta_0=\frac{-c^3}{3}+\frac{1}{3}, \qquad \beta_2=\frac{-c^2}{6}+\frac{1}{3},$$
$$\beta_1=\frac{c}{8}-\frac{c^3}{12}, \qquad \gamma_0=\frac{c^4}{36}-\frac{c^2}{12}+\frac{1}{8}, \qquad \gamma_2=\frac{c^2}{24}+\frac{1}{20}, \tag{57b}$$
$$\gamma_1=\frac{11c}{720}-\frac{c^3}{72}, \quad \mu_0=\frac{5c^4}{1080}-\frac{11c^2}{1080}+\frac{1}{180}, \quad \mu_2=\frac{-c^2}{240}+\frac{11}{2520},$$

and

$$g=1+\frac{c^2(\cos m-1)+ic(\sin m)}{1+(1-c^2)(\cos m-1)/3} \tag{57c}$$

$$\omega(\Delta t)\bar{\delta}=c\left[\frac{c}{24}(c^2-1)m^4+\cdots\right]$$

$$\omega(\Delta t)(a-\bar{\beta})=c[\tfrac{1}{180}(1-5c^2+5c^4)m^5+\cdots] \tag{57e}$$

Similarly, for the Euler–characteristic–Galerkin (ECG) algorithm

$$\alpha_1 = \frac{c}{2}, \qquad \beta_0 = \tfrac{1}{3}, \qquad \beta_2 = \frac{c^2}{6} + \frac{1}{3},$$

$$\beta_1 = \frac{c}{8} - \frac{c^2(\operatorname{sgn} a)}{12}, \quad \gamma_0 = \tfrac{1}{18}, \quad \gamma_2 = \frac{5c^2}{72} + \frac{1}{20}, \tag{58b}$$

$$\gamma_1 = \frac{11c}{720} + \frac{c^2(\operatorname{sgn} a)}{36}, \quad \mu_0 = \tfrac{1}{180}, \quad \mu_2 = \frac{c^2}{72} + \frac{11}{2520},$$

and

$$g = 1 + [c(\cos m - 1) + c^3(\cos m - 1)/3] - \mathrm{i}c(\sin m)[1 + c^2(\cos m - 1)/3], \tag{58c}$$

$$\omega(\Delta t)\bar{\delta} = c\left[-\frac{c}{24}(c-1)^2 m^4 + \cdots \right], \tag{58d}$$

$$\omega(\Delta t)(a - \bar{\beta}) = c[\tfrac{1}{180}(1 - 10c^2 + 15c^3 - 6c^4)m^5 + \cdots]. \tag{58e}$$

Therefore, both of these higher-order Galerkin algorithms also possess the unit CFL property, and for $c < 1$ are third-order accurate. Interestingly, for unit Courant number, the ETG algorithm is fifth-order accurate, whereas the ECG formula is sixth-order (the coefficient of m^5 also vanishes). Figure 5 summarizes the test case results for the ETG algorithm, and Figure 6 contains the linear test case results for the ECG algorithm. (A somewhat complicated 'recovery' process is required for the ECG algorithm, when applied to shocked flow predictions, the coding of which was deemed unnecessary for present purposes.) For ETG (Figure 5(a)) the linear, unsteady solution at $c = 0{\cdot}8$ is very accurate with no overshoot, minimal phase distortion (the nodal values are almost equidisposed across the wave), and with only the slightest indication of both a leading and lagging dispersion error. The linear steady-state ETG prediction is virtually identical to the Lax–Wendroff prediction, as expected since $\alpha_D = c/2$ in both cases. The unsteady, non-linear ETG solution (Figure 5(c)), is non-monotone, with both leading and lagging nominal $2\Delta x$ oscillations. The steady, non-linear solution is comparable to Lax–Wendroff, with a notable increase in oscillation magnitude. For the linear test problem comparisons, the ECG algorithm results for both the ($c = 0{\cdot}8$) linear unsteady case (Figure 6(a)), and the steady linear solution ($Pe = 40$, Figure 6(b)), are virtually indistinguishable from the ETG results.

Another form of a Taylor–Galerkin finite element algorithm has been developed by the CFD group at Swansea. Originally conceived as a Galerkin algorithm with added (Lapidus) dissipation[18–20] a recent reformulation has identified the underlying Taylor series conservation law statement.[21] The Swansea–Taylor–Galerkin (STG) finite element algorithm is an explicit two-step procedure, akin to Lax–Wendroff, that constitutes retention of a second term in the Taylor series, i.e. $\bar{\beta} = 1$ and $\bar{\alpha} = 0 = \bar{\gamma} = \bar{\mu}$ in equation (10), and $\theta = 0$ in equation (18). In terms of the parameters of equation (32), the STG algorithm is defined by

$$\alpha_A = 0 = \alpha_B = \alpha_C = \alpha_E = \theta,$$

$$\alpha_D = \frac{c}{2}. \tag{59a}$$

Thus, it is Lax–Wendroff algorithm with a mass matrix (recall that $\alpha_B \equiv 1/6$ in equations (55a) and (56a) removes the mass matrix contribution in equation (31) for Lax–Wendroff and donor-cell). With the definitions in equation (59a), the parameters of equations (44), (50) and (51) for the STG algorithm are

$$\alpha_1 = \frac{c}{2}, \qquad \beta_0 = \tfrac{1}{3}, \qquad \beta_2 = \tfrac{1}{3},$$

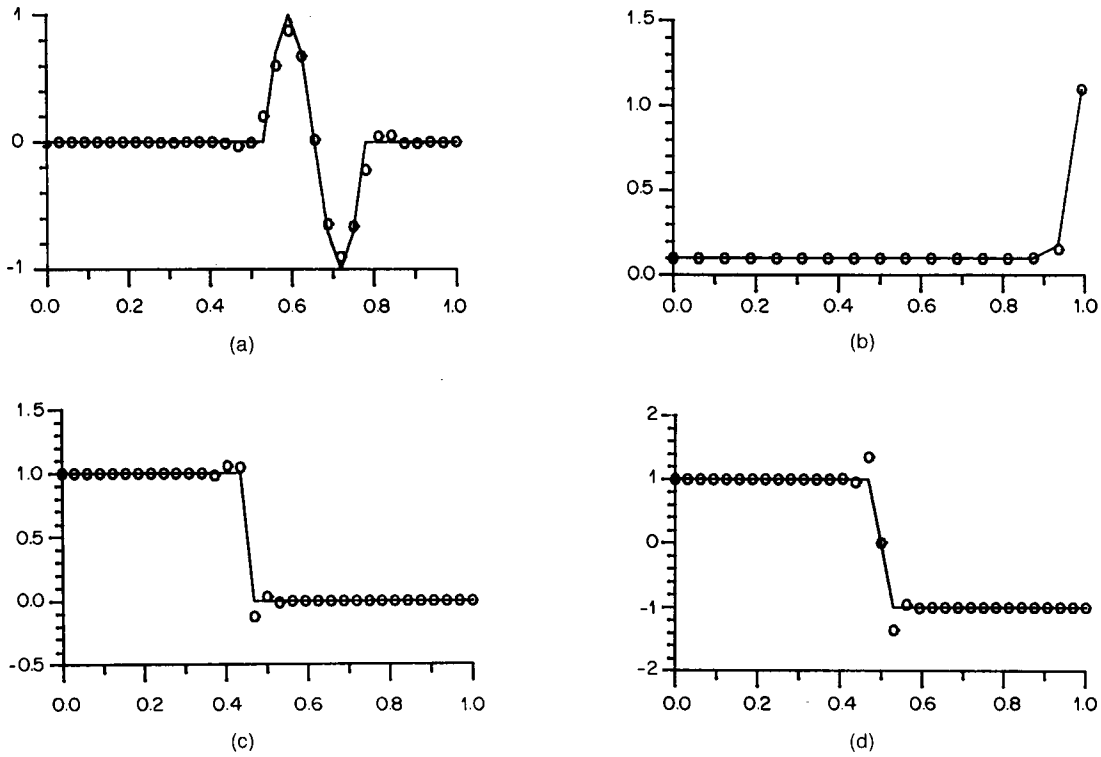

Figure 5. Euler–Taylor–Galerkin algorithm test problem solutions: (a) linear, unsteady, $c = 0{\cdot}8$; (b) linear, steady-state, $Pe = 40$; (c) non-linear, unsteady, $c = 0{\cdot}16$; (d) non-linear, steady-state

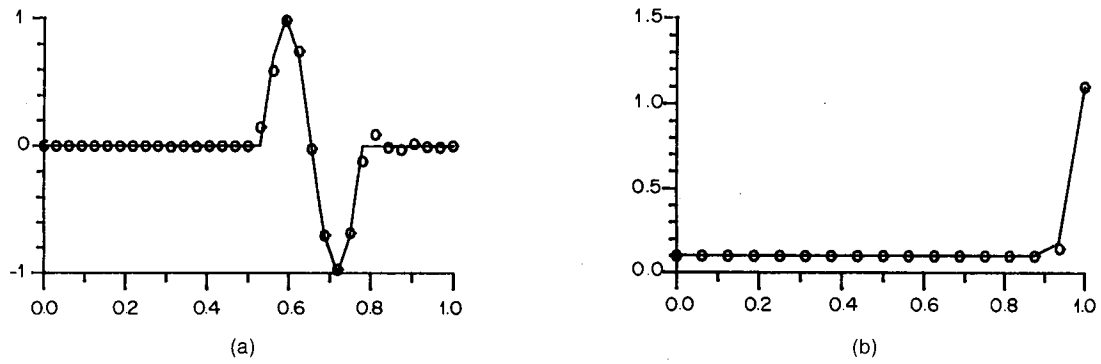

Figure 6. Euler–characteristic–Galerkin algorithm test problem solutions: (a) linear, unsteady, $c = 0{\cdot}8$; (b) linear, steady-state, $Pe = 40$

$$\beta_1 = \frac{c}{8}, \qquad \gamma_0 = \tfrac{1}{18}, \qquad \gamma_2 = \tfrac{1}{20}, \tag{59b}$$

$$\gamma_1 = \frac{11c}{720}, \quad \mu_0 = \tfrac{1}{180}, \quad \mu_2 = \tfrac{11}{2520},$$

$$g = 1 + \frac{c^2(\cos m - 1) - ic(\sin m)}{1 + (\cos m - 1)/3}, \tag{59c}$$

$$\omega(\Delta t)\bar{\delta} = c\left[\frac{c}{24}(3c^2 - 1)m^4 + \cdots\right], \tag{59d}$$

$$\omega(\Delta t)(a - \bar{\beta}) = c\left[-\left(\frac{c^2}{6}\right)m^3 + \tfrac{1}{180}(1 - \tfrac{15}{2}c^2 + 84c^4)m^5 + \cdots\right]. \tag{59e}$$

For stability, equation (59d) requires $c \leqslant 1\sqrt{3} \approx 0{\cdot}577$, a more severe constraint than that imposed by the choice of explicit integration. Figure 7 summarizes the STG algorithm test case problem solutions. The linear unsteady solution (Figure 7(a)), for $c = 0{\cdot}4$ confirms a modest level of artificial dissipation and significant leading phase error in distinction to Lax–Wendroff, (Figure 4(a)). This solution is notably poorer than both the ETG and ECG solutions, even though use of $c = 0{\cdot}4$ is a less severe test and requires twice the number of integration time steps. The linear, steady-state solution (Figure 7(b)), is indistinguishable from the entire class of Lax–Wendroff algorithms. In Figure 7(c) and 7(d), the non-linear unsteady and steady solutions are essentially indistinguishable from the ETG and Lax–Wendroff results, as the theoretical analysis predicts. Of course, the unsteady solution at $c = 0{\cdot}16$ requires about twice the number of integration steps for accuracy equivalent to Lax–Wendroff.

The family of Petrov–Galerkin algorithms

In distinction to the higher-order Galerkin methods, there have been published a number of so-called Petrov–Galerkin finite element algorithms, characterized by the choice of a test space distinct from the trial space; recall equations (13) and (14). Wahlbin,[1] Dendy[2] and Raymond and Garder[3] each published an unsteady dissipative Petrov–Galerkin algorithm in the mid-1970s. Hughes and Brooks[5] in 1979 published a steady-state algorithm termed 'Streamline upwind Petrov–Galerkin (SUPG)' and applied it to convection–diffusion problems. Tezduyar and Hughes[22] later extended the SUPG method to the Euler equations; Morton and Parrott[6] generalized to unsteady flows with an Euler–Petrov–Galerkin (EPG) algorithm, and Baker and Soliman[7] published an implicit unsteady Euler algorithm using a modified Raymond–Garder formulation. For these various algorithm constructions, viewing columns in Table I confirms the minimal distinctions amongst the class, which is uniformly characterized by introduction of an 'artificial' viscosity parameter v eligible for definition.

The explicit Euler–Petrov–Galerkin (EPG) and implicit Raymond–Garder (RG) formulations characterize the class; hence the direct comparison is of interest. The EPG algorithm is defined within the Taylor series, (equation (11)) by the constraints $\bar{\alpha} = 0 = \bar{\gamma} = \bar{\mu}$ and $\bar{\beta} \neq 0$. Within the Taylor weak statement, (equation (31)), the parameter set (equation 32) for EPG becomes

$$\begin{aligned} \alpha_A &= 0 = \alpha_C = \alpha_E = \theta, \\ \alpha_B &= \tfrac{1}{6}(1 - v), \\ \alpha_D &= \frac{v(\operatorname{sgn} a)}{2}. \end{aligned} \tag{60a}$$

Note that the 1/6 in α_B eliminates the mass matrix contribution in equation (31). The RG algorithm is established within the Taylor series, (equation (11)), by the specification $\bar{\alpha} = \bar{\beta}$ and $\bar{\gamma} = 0 = \bar{\mu}$. Thus, the RG parameters in equation (32) are

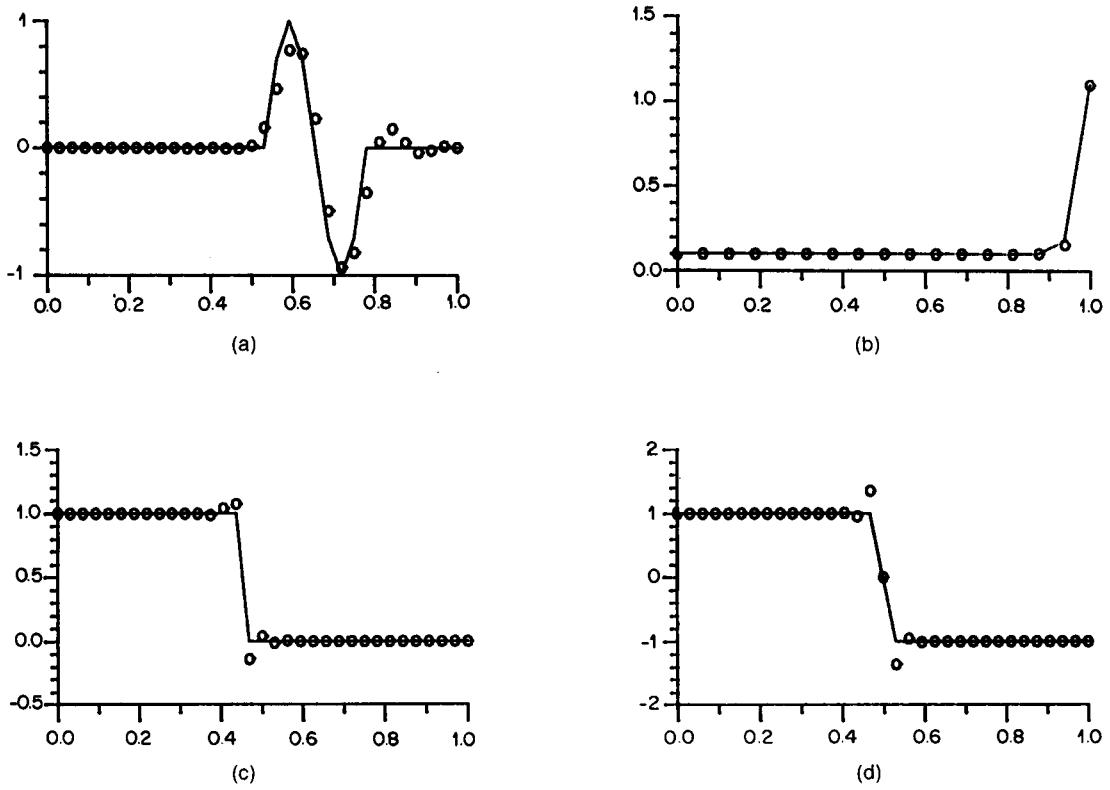

Figure 7. Swansea–Taylor–Galerkin algorithm test problem solutions: (a) linear, unsteady, $c = 0{\cdot}4$; (b) linear, steady-state, $Pe = 40$; (c) non-linear, unsteady, $c = 0{\cdot}16$; (d) non-linear, steady-state

$$\begin{aligned} \alpha_A &= c\theta - (\operatorname{sgn} a)v, \\ \alpha_B &= c\theta(\operatorname{sgn} a)v, \\ \alpha_C &= 0 = \alpha_E, \\ \alpha_D &= (\operatorname{sgn} a)v. \end{aligned} \tag{61a}$$

Completing the evaluations in equation (44) for EPG yields (for $\operatorname{sgn} a = 1$),

$$\begin{aligned} &\alpha_1 = \frac{v}{2}, \qquad \beta_0 = \frac{v}{3}, \qquad \beta_2 = \frac{(1+v)}{6}, \\ &\beta_1 = \frac{v(v+1/2)}{12}, \qquad \gamma_0 = \frac{v(v+1)}{36}, \qquad \gamma_2 = \frac{[v+(1/5)]}{24}, \\ &\gamma_1 = \frac{v(10v+1)}{720}, \qquad \mu_0 = \frac{(5v^2+v+4)}{1080}, \qquad \mu_2 = \frac{11}{2520} - \frac{(1-v)}{240}. \end{aligned} \tag{60b}$$

Therefore, the Fourier solution expressions for EPG become (equations (42), (50) and (51))

$$g = 1 + \frac{c(v(\cos m - 1) - \mathrm{i}(\sin m))}{1 + \frac{v}{3}(\cos m - 1)}, \tag{60c}$$

$$\omega(\Delta t)\bar{\delta} = c\left\{\frac{1}{2}(c-v)m^2 + \left[v\left(\frac{c^2}{4}+\frac{c}{6}+\frac{1}{24}\right) - \frac{v^2}{12} - \frac{c}{6} - \frac{c^3}{8}\right]m^4 + \cdots\right\}, \tag{60d}$$

$$\omega(\Delta t)(a-\bar{\beta}) = c\left[\left(\frac{1}{6}+\frac{c^2}{3}-\frac{v(3c+1)}{6}\right)m^3 + \cdots\right]. \tag{60e}$$

Completing the evaluations in equation (44) for RG yields (for $\operatorname{sgn} a = 1$),

$$\begin{aligned}
&\alpha_1 = \frac{c\theta}{2}, && \beta_0 = \tfrac{1}{3} - (c\theta)^2 - v^2,\\
&\beta_1 = c\theta(\tfrac{1}{3} - v^2) - \frac{v}{12}, && \gamma_0 = (c\theta)^2(v^2 - \tfrac{1}{3}) + \frac{c\theta v}{6} + \frac{1}{18} - \frac{v^2}{3},\\
&\gamma_1 = c\theta\left(\frac{2}{45} - \frac{v^2}{6}\right) - \frac{v}{72}, && \mu_0 = (c\theta)^2\frac{[v^2 - (4/15)]}{6} + \frac{c\theta v}{36} + \frac{(1-8v^2)}{180},\\
&\beta_2 = \tfrac{1}{3} - v^2, &&\\
&\gamma_2 = \frac{[(1/5) - v^2]}{4}, &&\\
&\mu_2 = \frac{[(11/63) - v^2]}{40}. &&
\end{aligned} \tag{61b}$$

Hence, for equations (42), (50) and (51)

$$\begin{aligned}
g &= 1 + \frac{c[2v(\cos m - 1) - \mathrm{i}(\sin m)]}{1 + [(1/3) - 2c\theta v](\cos m - 1) + \mathrm{i}(\sin m)(c\theta - v)},\\
&= \frac{1 + [(1/3) + 2cv(1-\theta)](\cos m - 1) - \mathrm{i}(\sin m)(1 + v - c\theta)}{1 + [(1/3) - 2c\theta v](\cos m - 1) + \mathrm{i}(\sin m)(c\theta - v)},
\end{aligned} \tag{61c}$$

$$\omega(\Delta t)\bar{\delta} = c\left\{c[(1/2) - \theta]m^2 + \left[c^3\left(\theta^3 - \theta^2 + \frac{\theta}{2} - \frac{1}{8}\right) - \frac{v}{12}\right]m^4 + \cdots\right\}, \tag{61d}$$

$$\omega(\Delta t)(a-\bar{\beta}) = c[c^2(\theta^2 - \theta + \tfrac{1}{3})m^3 + \cdots]. \tag{61e}$$

Although the appearance of terms in Table I conveys the impression that these two algorithms share much in common, equations (60) and (61) firmly quantify the substantial distinctions that exist. The EPG algorithm is unstable for $c > v$, and only first order accurate unless $v = c$. For $v = c$, stability requires that $c \leqslant 1/3$ for positive damping in the order m^4 term (equation (6d)). Finally, v is bounded below unity from the original definition of the test space for EPG. Conversely, the RG algorithm is identical to Bubnov–Galerkin to order m^4, and for $\theta = 1/2$ is third-order accurate and stable independent of v. For $\theta = 1/2$, damping in the m^4 term is due only to v and is positive for any $v > 0$. The definition $v \equiv (15)^{-1/2}$, as originally determined 'optimal' by Raymond and Garder,[3] yields their predicted value $\bar{\delta} = a(\Delta x)^3/12\sqrt{15}$. For this value of v, their analysis incorrectly predicted higher order phase accuracy, based on a semi-discrete Fourier analysis.

The computed test case results are summarized in Figures 8 and 9 for the EPG and RG algorithms, respectively. For the linear unsteady problem, the EPG solution for $c = 0{\cdot}32 = v$ shows a large lagging phase yielding a distorted dissipation and a large amplitude trailing wake (Figure 8(a)). Setting $v = 0{\cdot}5$ and $c = 0{\cdot}32$ (the stability limit) introduces a large dissipation on

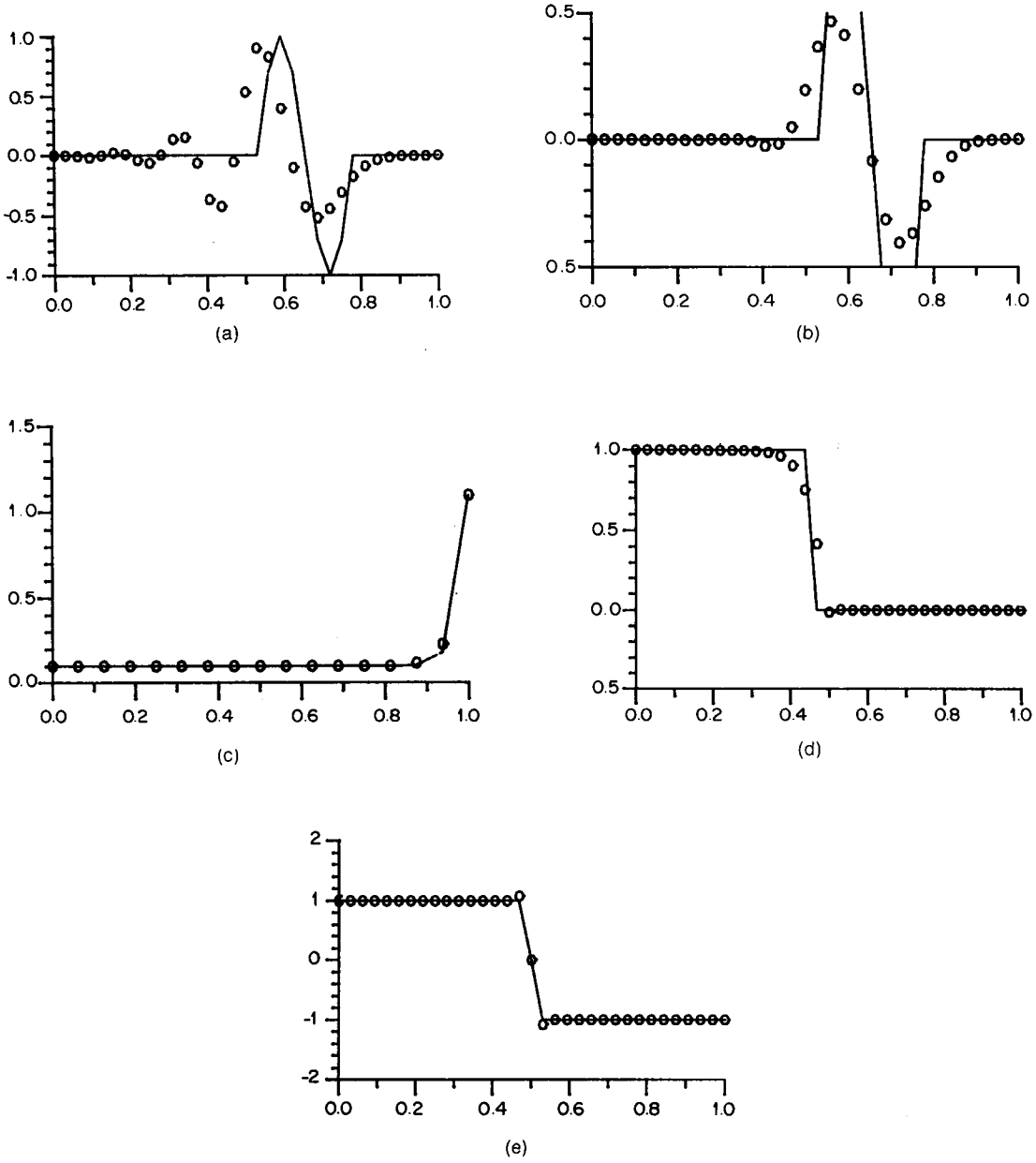

Figure 8. Euler–Petrov–Galerkin algorithm test problem solutions: (a) linear, unsteady, $c = 0{\cdot}32$, $v = 0{\cdot}32$; (b) linear, unsteady, $c = 0{\cdot}32$, $v = 0{\cdot}5$; (c) linear, steady-state, $Pe = 40$, $v = 0{\cdot}5$; (d) non-linear, unsteady, $c = 0{\cdot}32$, $v = 0{\cdot}95$, $\theta = 1$; (e) non-linear, steady-state, $v = 0{\cdot}95$.

top of the large phase error (Figure 8(b)). For the steady problem at $Pe = 40$, the $v = 0{\cdot}5$ solution is in close agreement with the analytical solution (Figure 8(c)). For the non-linear unsteady problem (Figure 8(d)), the EPG solution for $v = 0{\cdot}95$, $c = 0{\cdot}32$ (as stabilized using $\theta = 1$) yields an almost monotone but diffused solution. The steady, non-linear EPG solution for $v = 0{\cdot}95$ appears essentially identical to donor cell, in agreement with its being first-order accurate.

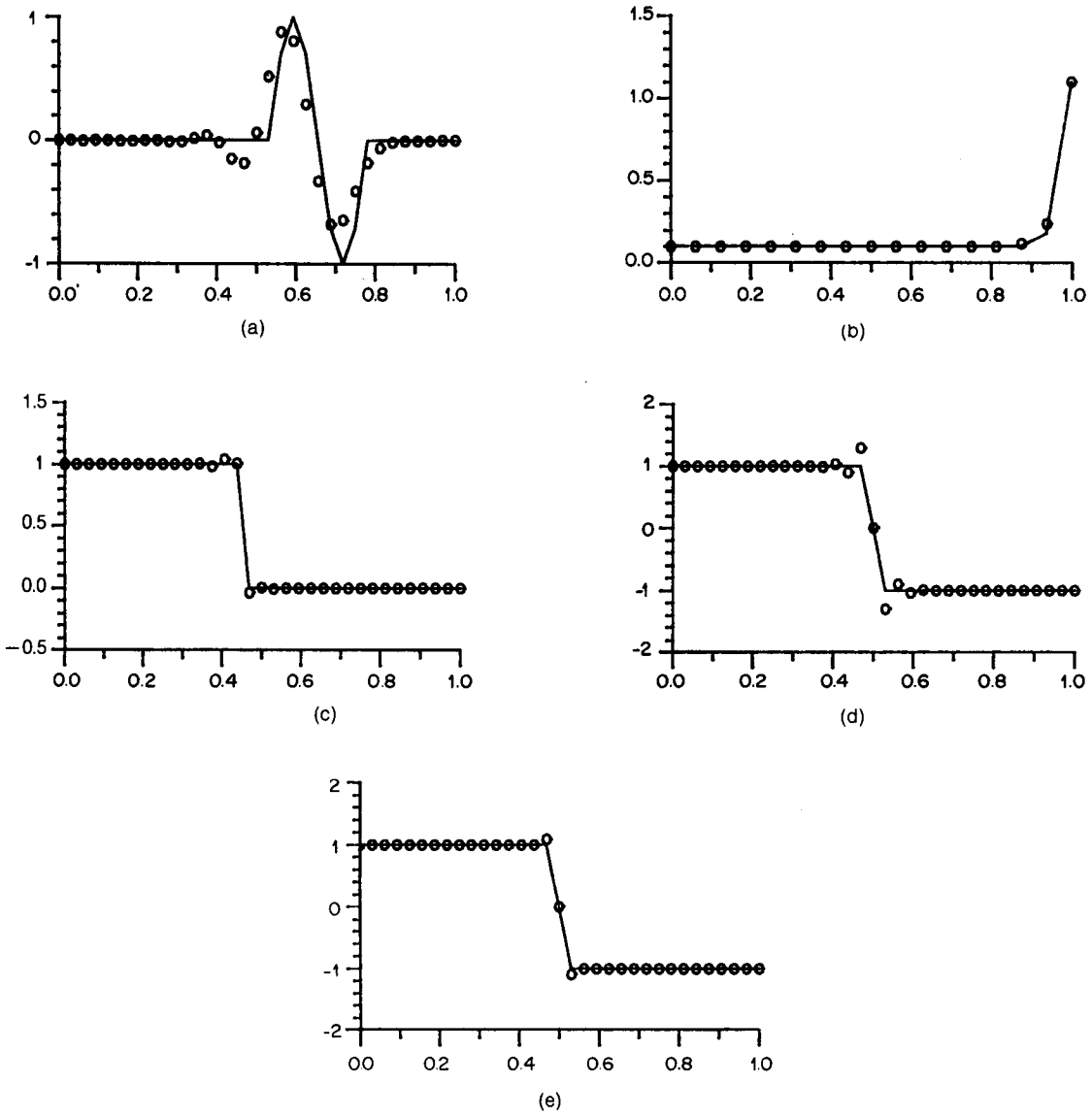

Figure 9. Raymond–Garder finite element algorithm test problem solutions: (a) linear, unsteady, $\theta = 0{\cdot}5$, $c = 0{\cdot}8$, $v = 1/\sqrt{15}$; (b) linear, steady-state, $\theta = 0{\cdot}5$, $1{\cdot}0$, $Pe = 40$, $v = 1/\sqrt{15}$; (c) non-linear, unsteady, $\theta = 1{\cdot}0$, $c = 0{\cdot}32$, $v = 1/\sqrt{15}$; (d) non-linear, steady-state, $\theta = 0{\cdot}5$, $1{\cdot}0$, $v = 1/\sqrt{15}$; (e) non-linear, steady-state, $\theta = 0{\cdot}5$, $1{\cdot}0$, $v = 2/\sqrt{15}$

The RG algorithm solution for the linear unsteady problem at $c = 0{\cdot}8$, for $\theta = 1/2$ and $v = 1/\sqrt{15}$ (Figure 9(a)) shows no over- or undershoot, with the same lagging phase distortion but reduced trailing wake when compared to Bubnov–Galerkin (Figure 2(a)). The steady linear RG solution is independent of θ, and for $v = 1/\sqrt{15}$ and $Pe = 40$ is in good agreement with the exact solution (Figure 9(b)). The non-linear, unsteady solution for $c = 0{\cdot}32$ shows modest overshoot for $\theta = 1$, $v = 1/\sqrt{15}$, which is also an improvement over Bubnov–Galerkin; recall Figure 2(e). The unsteady non-linear solution is also θ-independent, and Figure 9(d) and 9(e) show the influence of the level of v in modifying the non-monotone character between that of Lax–Wendroff and donor cell.

SUMMARY AND CONCLUSIONS

A Taylor weak-statement finite element numerical solution algorithm has been derived for application to hyperbolic conservation law systems in computational fluid dynamics. For a linear basis implementation, and a Galerkin test space definition, a theoretical stability analysis has been completed for a one-dimensional scalar equation. The results of this analysis have permitted direct theoretical comparison of a variety of dissipative algorithms published in the finite difference and finite element literature. Linear and non-linear, unsteady and steady test problems were defined, and the various dissipative algorithm solutions directly compared to quantify relative performance.

A critical assessment of these results confirms that none of the published algorithms satisfactorily meets the multiple requirements of accuracy, efficiency and monotonicity for the entire test problem family. This is not surprising, since none of these algorithms were specifically constructed according to a norm that would guarantee, or even promote, such optimum performance. It is quite evident that the Taylor weak-statement, based on a Galerkin weighting criterion, does provide a functional form upon which such an optimized analysis could be performed. Such a project is under way, as well as an extension of the analysis framework to encompass an even broader CFD algorithm class, including those characterized by upwinding,[23] flux vector splittings,[24] flux limiters[25,26] and with fourth-order added dissipation mechanisms.[27]

ACKNOWLEDGEMENTS

The authors wish to acknowledge the contribution of computer resources by the University of Tennessee Computing Center and the graduate student financial support provided by the corporate sustaining members of the Computational Fluid Dynamics Laboratory. This work was partially supported by the NASA Langley Research Center under grant NAG1-319, which is gratefully acknowledged.

APPENDIX I

Consider the evaluation of the integral (equation (27)) in the form

$$S_e(E_e) \equiv S_e\left(h_e^3 \int_{\Omega_e} \{N_2\}_x \{N_1\}_{xx}^{\mathrm{T}} \, \mathrm{d}x \right), \tag{62}$$

where $\{N_2\}$ is the quadratic basis function of the test space and $\{N_1\}$ is the linear basis function of the trial space. Defining the natural co-ordinate $\zeta = \bar{x}/2h_e$, where h_e is the measure of the one-dimensional linear basis element, one obtains the relations

$$\{N_1\} = \begin{Bmatrix} 1-2\zeta \\ 2\zeta \end{Bmatrix},$$

$$\{N_1\}_x = \frac{1}{h_e} \begin{Bmatrix} -1 \\ 1 \end{Bmatrix},$$

$$\{N_2\} = \begin{Bmatrix} (1-\zeta) & (1-2\zeta) \\ 4\zeta & (1-\zeta) \\ -\zeta & (1-2\zeta) \end{Bmatrix},$$

$$\{N_2\}_x = \frac{1}{2h_e}\begin{Bmatrix} -3+4\zeta \\ 4-8\zeta \\ -1+4\zeta \end{Bmatrix},$$

$$\{N_2\}_{xx} = \frac{1}{h_e^2}\begin{Bmatrix} 1 \\ -2 \\ 1 \end{Bmatrix}.$$

The integral defined in equation (62) can be re-expressed using integration by parts, yielding

$$h_e^3 \int_{\Omega_e} \{N_2\}_x \{N_1\}_{xx}^{\mathrm{T}} \, \mathrm{d}x = h_e^3 \oint_{\partial\Omega_e} \{N_2\}_x \{N_1\}_x^{\mathrm{T}} \cdot \hat{n} \, \mathrm{d}\tau - h_e^3 \int_{\Omega_e} \{N_2\}_{xx} \{N_1\}_x^{\mathrm{T}} \, \mathrm{d}x. \tag{63}$$

in regions of smooth flow, the surface integral in equation (63) is usually assumed to vanish. Since $\{N_2\}$ requires three nodal coefficients for interpolation, whereas $\{N_1\}$ needs only two coefficients, expand the rank accordingly to yield

$$\{N_1\}^{\mathrm{T}} \equiv \begin{cases} \{1-2\zeta, 2\zeta, 0\}, & \text{for } a_e > 0, \\ \{0, 1-2\zeta, 2\zeta\}, & \text{for } a_e < 0, \end{cases}$$

where a_e is the element convection velocity. Referring to Figure 10, and for a uniform discretization (h_e = constant), the evaluation of equation (63) is computed as follows:

Case (i): $a_e > 0$

$$\begin{aligned} h_e^3 \int_{\Omega_e} \{N_2\}_x \{N_1\}_{xx}^{\mathrm{T}} \, \mathrm{d}x &\equiv -h_e^3 \int_0^{h_e} \{N_2\}_{xx} \{N_1\}_x^{\mathrm{T}} \, \mathrm{d}x \\ &= -h_e^3 \int_0^{h_e} \frac{1}{h_e^2} \begin{Bmatrix} 1 \\ -2 \\ 1 \end{Bmatrix} \frac{1}{h_e} \{-1 \quad 1 \quad 0\} \, \mathrm{d}x \\ &= h_e \begin{bmatrix} 1 & -1 & 0 \\ -2 & 2 & 0 \\ 1 & -1 & 0 \end{bmatrix}. \end{aligned} \tag{64}$$

Case (ii): $a_e < 0$

$$\begin{aligned} h_e^3 \int_{\Omega_e} \{N_2\}_x \{N_1\}_{xx}^{\mathrm{T}} \, \mathrm{d}x &\equiv -h_e^3 \int_0^{h_e} \{N_2\}_{xx} \{N_1\}_x^{\mathrm{T}} \, \mathrm{d}x \\ &= -h_e^3 \int_0^{h_e} \frac{1}{h_e^2} \begin{Bmatrix} 1 \\ -2 \\ 1 \end{Bmatrix} \frac{1}{h_e} \{0 \quad -1 \quad 1\} \, \mathrm{d}x \end{aligned}$$

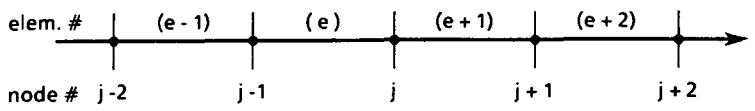

Figure 10. Generic discretization of the x-axis

$$= h_e \begin{bmatrix} 0 & 1 & -1 \\ 0 & -2 & 2 \\ 0 & 1 & -1 \end{bmatrix}. \tag{65}$$

Hence, using $\{N_2\}$ and integration by parts, we obtain the definition given before as equation (27)

$$S_e(E_e) \equiv S_e\left(h_e^3 \int_{R_e^1} \{N_2\}_x \{N_1\}_{xx}^{\mathrm{T}} \mathrm{d}x \right) = \begin{cases} h_e \begin{bmatrix} 1 & -1 & 0 \\ -2 & 2 & 0 \\ 1 & -1 & 0 \end{bmatrix}, & a > 0, \\ h_e \begin{bmatrix} 0 & 1 & -1 \\ 0 & -2 & 2 \\ 0 & 1 & -1 \end{bmatrix}, & a < 0. \end{cases}$$

Alternatively, since the integral

$$\int_{\Omega_e} \{N_2\}_x \{N_1\}_{xx}^{\mathrm{T}} \mathrm{d}\tau \tag{66}$$

vanishes identically, as $\{N_1\}$ cannot support two x-derivatives, we must have

$$\oint_{\partial\Omega_e} \{N_2\}_x \{N_1\}_x^{\mathrm{T}} \cdot \hat{n} \, \mathrm{d}\tau = \int_{\Omega_e} \{N_2\}_{xx} \{N_1\}_x^{\mathrm{T}} \mathrm{d}x. \tag{67}$$

For $a_e > 0$,

$$\begin{aligned} h_e^3 \oint_{\partial\Omega_e} \{N_2\}_x \{N_1\}_x^{\mathrm{T}} \cdot \hat{n} \, \mathrm{d}\tau &= \frac{h_e^3}{2h_e} \begin{Bmatrix} -3+4\zeta \\ 4-8\zeta \\ -1+4\zeta \end{Bmatrix} \frac{1}{h_e} \{-1 \quad 1 \quad 0\} \Big|_0^{1/2} \\ &= h_e \begin{bmatrix} -1 & 1 & 0 \\ 2 & -2 & 0 \\ -1 & 1 & 0 \end{bmatrix} \\ &= h^3 \int \{N_2\}_x \{N_1\}_{xx}^{\mathrm{T}} \mathrm{d}x. \end{aligned} \tag{68}$$

For $a_e < 0$,

$$\begin{aligned} h_e^3 \oint_{\partial\Omega_e} \{N_2\}_x \{N_1\}_x^{\mathrm{T}} \cdot \hat{n} \, \mathrm{d}\tau &= \frac{h_e^3}{2h_e} \begin{Bmatrix} -3+4\zeta \\ 4-8\zeta \\ -1+4\zeta \end{Bmatrix} \frac{1}{h_e} \{0 \quad -1 \quad 1\} \Big|_0^{1/2} \\ &= h_e \begin{bmatrix} 0 & -1 & 1 \\ 0 & 2 & -2 \\ 0 & -1 & 1 \end{bmatrix} \\ &= h^3 \int_{R_e^1} \{N_2\}_x \{N_1\}_{xx}^{\mathrm{T}} \mathrm{d}x, \end{aligned} \tag{69}$$

which again recovers equation (27).

As a final construction using only $\{N_1\}$, consider introduction of a new element degree of freedom $\{\mathrm{QX}\}_e$ defined as (recall Figure 10)

$$\{\mathrm{QX}\}_e = \begin{cases} \dfrac{1}{h_e}\begin{Bmatrix} Q_{j-1}-Q_{j-2} \\ Q_j - Q_{j-1} \end{Bmatrix}_e, & a>0, \\ \dfrac{1}{h_e}\begin{Bmatrix} Q_j - Q_{j-1} \\ Q_{j+1}-Q_j \end{Bmatrix}_e, & a<0. \end{cases} \tag{70}$$

For constant a, the last term in the Taylor weak statement (equation (25)) can then be written as

$$\int_{\Omega_e} \{N_1\}_x (\{N_1\}^{\mathrm{T}}\{Q\}_e)_{xx}\,\mathrm{d}x = \frac{1}{h_e}\int_{\Omega_e} \{N_1\}_x \{N_1\}_x^{\mathrm{T}}\{\mathrm{QX}\}_e\,\mathrm{d}x. \tag{71}$$

Equation (71), upon assembly over the element pair sharing node j (Figure 10), for a uniform discretization then yields the expression $\delta^2\Delta_{\mp}Q_j$ as follows; for $a>0$ and on element e,

$$\begin{aligned} \int_{\Omega_e} \{N\}_x\{N\}_x^{\mathrm{T}}\,\mathrm{d}x\{Q\}_e &= \frac{1}{h_e}\begin{bmatrix} 1 & -1 \\ -1 & 1 \end{bmatrix}\frac{1}{h_e}\begin{Bmatrix} Q_{j-1}-Q_{j-2} \\ Q_j - Q_{j-1} \end{Bmatrix} \\ &= \frac{1}{h_e^2}\begin{Bmatrix} -Q_{j-2}+2Q_{j-1}-Q_j \\ Q_{j-2}-2Q_{j-1}+Q_j \end{Bmatrix}_e, \end{aligned} \tag{72}$$

whereas for the adjacent element, $e+1$,

$$\int_{\Omega_e} \{N\}_x\{N\}_x^{\mathrm{T}}\,\mathrm{d}x\{Q\}_{e+1} = \frac{1}{h^2}\begin{Bmatrix} -Q_{j-1}+2Q_j-Q_{j+1} \\ Q_{j-1}-2Q_j+Q_{j+1} \end{Bmatrix}_{e+1}. \tag{73}$$

Thus, upon assembly of the element contributions, we have for the subject term

$$S_{e,e+1}\int_{\Omega_e} \{N_1\}_x(\{N_1\}^{\mathrm{T}}\{Q\}_e)_{xx}\,\mathrm{d}x = \frac{1}{h^2}\{Q_{j-2}-3Q_{j-1}+3Q_j-Q_{j+1}\}^{\mathrm{T}},$$

which, upon extraction of a common multiplier Q_j confirms the form of equation (29) as

$$S_e(E_e) = \begin{cases} \dfrac{-1}{h^2}\delta^2\Delta_-, & a>0, \\ \dfrac{-1}{h^2}\delta^2\Delta_+, & a<0. \end{cases} \tag{74}$$

Q.E.D.

APPENDIX II

From equation (42), we write the amplification factor g as follows:

$$\begin{aligned} g-1 &= c(R_2-\mathrm{i}I_2)/(R_1+\mathrm{i}I_1) \\ &= c[(R_1R_2-I_1I_2)-\mathrm{i}(R_1I_2+R_2I_1)]/(R_1^2+I_1^2), \end{aligned} \tag{75}$$

where

$$\begin{aligned} R_1 &= 1+(\tfrac{1}{3}-2\alpha_{\mathrm{B}})(\cos m-1)-2(\operatorname{sgn} a)\alpha_{\mathrm{C}}(\cos m-1)^2, \\ I_1 &= (\sin m)[\alpha_{\mathrm{A}}+2\alpha_{\mathrm{C}}(\cos m-1)], \\ R_2 &= 2\alpha_{\mathrm{D}}(\cos m-1)+2(\operatorname{sgn} a)\alpha_{\mathrm{E}}(\cos m-1)^2, \\ I_2 &= (\sin m)[1+2\alpha_{\mathrm{E}}(\cos m-1)]. \end{aligned} \tag{76}$$

One has the following series expansions for sines and cosines

$$\cos m - 1 = -\frac{m^2}{2}\left(1 - \frac{m^2}{12} + \frac{m^4}{360} - \frac{m^6}{20{,}160} + \cdots\right),$$

$$\sin m = m\left(1 - \frac{m^2}{6} + \frac{m^4}{120} - \frac{m^6}{5040} + \frac{m^8}{362{,}880} + \cdots\right),$$

$$(\cos m - 1)^2 = \frac{m^4}{4}\left(1 - \frac{m^2}{6} + \frac{m^4}{80} - \cdots\right),$$

$$\sin^2 m = m^2\left(1 - \frac{m^2}{3} + \frac{2}{45}m^4 - \frac{m^6}{315} + \cdots\right),$$

$$(\sin m)(\cos m - 1) = -\frac{m^3}{2}\left(1 - \frac{m^2}{4} + \frac{m^4}{40} - \cdots\right). \tag{77}$$

Expanding R_1, I_1, R_2 and I_2 (equation (76)) in terms of powers of m then yields

$$R_1 = 1 - (\tfrac{1}{6} - \alpha_B)m^2 + \left[\frac{1}{12} - \frac{\alpha_B}{2} - (\operatorname{sgn} a)\frac{\alpha_C}{2}\right]m^4 - \left(\frac{1}{2160} - \frac{\alpha_B}{360} - (\operatorname{sgn} a)\frac{\alpha_C}{12}\right)m^6 + \cdots,$$

$$I_1 = \alpha_A m - \left(\frac{\alpha_A}{6} + \alpha_C\right)m^3 + \left(\frac{\alpha_A}{120} + \frac{\alpha_C}{4}\right)m^5 - \left(\frac{\alpha_A}{5040} + \frac{\alpha_C}{40}\right)m^7 + \cdots,$$

$$R_2 = -\alpha_D m^2 + \left[\frac{\alpha_D}{12} + (\operatorname{sgn} a)\frac{\alpha_E}{2}\right]m^4 - \left[\frac{\alpha_D}{360} + (\operatorname{sgn} a)\frac{\alpha_E}{12}\right]m^6 + \left[\frac{\alpha_D}{20{,}160} + (\operatorname{sgn} a)\frac{\alpha_E}{160}\right]m^8 - \cdots,$$

$$I_2 = m - (\tfrac{1}{6} + \alpha_E)m^3 + \left(\frac{1}{120} + \frac{\alpha_E}{4}\right)m^5 - \left(\frac{1}{5040} + \frac{\alpha_E}{40}\right)m^7 + \cdots. \tag{78}$$

Thus, we can establish the expressions,

$$R_1^2 + I_1^2 = 1 - \beta_0 m^2 + \gamma_0 m^4 - \mu_0 m^6 + \cdots,$$

$$R_1 R_2 - I_1 I_2 = m^2(-\alpha_1 + \beta_1 m^2 - \gamma_1 m^4 + \cdots),$$

$$R_1 I_2 + R_2 I_1 = m(1 - \beta_2 m^2 + \gamma_2 m^4 - \mu_2 m^6 + \cdots), \tag{79}$$

The parameters β, γ, μ,... then lead to the definitions

$$\frac{R_1 R_2 - I_1 I_2}{R_1^2 + I_1^2} = \frac{m^2(-\alpha_1 + \beta_1 m^2 - \gamma_1 m^4 + \cdots)}{1 - \beta_0 m^2 + \gamma_0 m^4 - \mu_0 m^6 + \cdots}$$

$$= -\alpha_1 m^2 + (\beta_1 - \beta_0\alpha_1)m^4 - [(\gamma_1 - \gamma_0\alpha_1) - \beta_0(\beta_1 - \beta_0\alpha_1)]m^6 + O(m^8), \tag{80}$$

$$\frac{R_1 I_2 + R_2 I_1}{R_1^2 + I_1^2} = \frac{m(1 - \beta_2 m^2 + \gamma_2 m^4 - \mu_2 m^6 + \cdots)}{1 - \beta_0 m^2 + \gamma_0 m^4 - \mu_0 m^6 + \cdots}$$

$$= m - (\beta_2 - \beta_0)m^3 + [(\gamma_2 - \gamma_0) - \beta_0(\beta_2 - \beta_0)]m^5 - [(\mu_2 - \mu_0) - \gamma_0(\beta_2 - \beta_0) - \beta_0(\gamma_2 - \gamma_0) + \beta^2(\beta_2 - \beta_0)]m^7 + O(m^9). \tag{81}$$

Substitution of equations (80) and (81) into equation (75) then yields equation (43):

$$g = 1 + c\{-\alpha_1 m^2 + (\beta_1 - \beta_0\alpha_1)m^4 - [(\gamma_1 - \gamma_0\alpha_1) - \beta_0(\beta_1 - \beta_0\alpha_1)]m^6 + O(m^8)\}$$
$$- ic\{m - (\beta_2 - \beta_0)m^3 + [(\gamma_2 - \gamma_0) - \beta_0(\beta_2 - \beta_0)]m^5$$
$$- [(\mu_2 - \mu_0) - \gamma_0(\beta_2 - \beta_0) - \beta_0(\gamma_2 - \gamma_0) + \beta^2(\beta_2 - \beta_0)]m^7 + O(m^9)\} \quad (43)$$

Q.E.D.

REFERENCES

1. L. B. Wahlbin, 'A dissipative Galerkin method applied to some quasi-linear hyperbolic equations', *R.A.I.R.O.*, **8,** 109–117 (1974).
2. J. E. Dendy, 'Two methods of Galerkin type achieving optimum L^2 rates of convergence for first-order hyperbolics', *SIAM J. Numerical Analysis*, **11,** 637–653 (1974).
3. W. H. Raymond and A. Garder, 'Selective damping in a Galerkin method for solving wave problems with variable grids', *Monthly Weather Review*, **104,** 1583–1590 (1976).
4. J. C. Heinrich, P. S. Huyakorn, O. C. Zienkiewicz and A. R. Mitchell, 'An "upwind" finite element scheme for two-dimensional convective transport equation', *Int. j. numer. methods eng.*, **11,** 134–143 (1977).
5. T. J. R. Hughes and A. N. Brooks, 'A multidimensional upwind scheme with no crosswind diffusion', in T. J. R. Hughes (ed.), *Finite Element Methods for Convection Dominated Flows*, ASME, AMD-34, New York, 1979, pp. 19–35.
6. K. W. Morton and A. K. Parrott, 'Generalized Galerkin methods for first order hyperbolic equations', *J. Comp. Phys.*, **36,** 249–270 (1980).
7. A. J. Baker and M. O. Soliman, 'A finite element algorithm for computational fluid dynamics', *AIAAJ.*, **21,** 816–827 (1983).
8. K. W. Morton, 'Characteristic Galerkin methods for hyperbolic problems', *Proc. 5th GAMM Conf. Num. Mtd. Fluid Mechanics*, Rome, 1983.
9. J. Donea, 'A Taylor–Galerkin method for convective transport problems', *Int. j. numer. methods eng.*, **20,** 101–119 (1984).
10. A. J. Baker, 'On a penalty finite element algorithm for high speed flow', *J. Comp. Mtd. Appl. Mech. and Eng.*, **51,** 395–420 (1985).
11. T. J. R. Hughes and T. E. Tezduyar, 'Finite element methods for the compressible Euler equations', *Comp. Mtd. Appl. Mech. and Engr.*, **45,** 217–284 (1984).
12. R. Courant, E. Isaacson and M. Rees, 'On the solution of nonlinear hyperbolic differential equations', *Comm. Pure Appl. Math.*, **5,** 243–255 (1952).
13. P. D. Lax and B. Wendroff, 'Systems of conservation laws', *Comm. Pure Appl. Math.*, **13,** 217–237 (1960).
14. J. Donea, S. Giuliani, H. Laval and L. Quartapelle, 'Time-accurate solution of advection diffusion problems by finite elements', *Comp. Mtd. Appl. Mech. and Engr.*, **45,** 123–145 (1984).
15. V. Selmin, J. Donea and L. Quartapelle, 'Taylor–Galerkin method for non-linear hyperbolic equations', in R. W. Lewis, E. Hinton, P. Bettess and B. A. Schrefler (eds), *Proc. Int. Conf. Num. Mtd. for Transient and Coupled Problems*, Pineridge Press, Swansea, 1984.
16. V. Selmin, J. Donea and L. Quartapelle, 'Finite element method for nonlinear hyperbolic problems', *Comp. Mtd. Appl. Mech. and Engr.*, **52,** 817–845 (1985).
17. K. W. Morton, 'Generalized Galerkin methods for hyperbolic problems', *Comp. Mtd. Appl. Mech. and Engr.*, **52,** 847–871 (1985).
18. R. Löhner, K. Morgan and O. C. Zienkiewicz, 'The solution of non-linear hyperbolic equation systems by the finite element method', *Int. j. numer. methods fluids*, **4,** 1043–1063 (1984).
19. R. Löhner, K. Morgan and O. C. Zienkiewicz, 'The use of domain splitting with an explicit hyperbolic solver', *Comp. Mtd. Appl. Mech. and Engr.*, **45,** 313–329 (1984).
20. R. Löhner, K. Morgan and O. C. Zienkiewicz, 'An adaptive finite element procedure for compressible high speed flows', *Comp. Meth. Appl. Mech. and Engr.*, **51,** 441–465 (1985).
21. R. Löhner, K. Morgan, J. Peraire and O. C. Zienkiewicz, 'Finite element methods for high speed flows', *Proc. AIAA 7th Comp. Fluid Dyn. Conf.*, Cincinatti, OH, 1985, pp. 403–410.
22. T. E. Tezduyar and T. R. J. Hughes, 'Development of time-accurate finite element techniques for first order hyperbolic systems with particular emphasis on the compressible Euler equations', Standford University Report, 1983.
23. R. F. Warming and R. M. Beam, 'Upwind 2nd order difference schemes and applications in unsteady aerodynamic flows', *Proc. AIAA 2nd Comp. Fluid Dynamics Conference*, Hartford, CT, 1975, pp. 17–28.
24. W. K. Anderson, J. L. Thomas and B. van Leer, 'A comparison of finite volume flux vector splittings for the Euler equations', *Technical Paper AIAA-85-0122*, 1985.
25. T. J. R. Hughes and M. Mallet, 'A high precision finite element method for shock tube calculations', in R. H. Gallagher, G. F. Carey, J. T. Oden and O. C. Zienkiewicz (eds), *Finite Elements in Fluids, Vol. 6*, Wiley, Chichester 1986.
26. P. L. Roe, 'Approximate Reimann solvers, parameter vectors and difference schemes', *J. Comp. Physics*, **43,** 357–372 (1983).
27. R. M. Beam and R. F. Warming, 'An implicit finite difference algorithm for hyperbolic systems in conservation law form', *J. Comp. Physics*, **22,** 87–110 (1976).